The Role of Active Site Flexible Loops in Catalysis and of Zinc in Conformational Stability of Bacillus cereus 569/H/9 β-Lactamase

Caroline Montagner, Michael Nigen, Olivier Jacquin, Nicolas Willet, Mireille Dumoulin, Andreas Ioannis Karsisiotis, Gordon C. K. Roberts, Christian Damblon, Christina Redfield, André Matagne

Uncoupling proteins 1 and 2 (UCP1 and UCP2) from *Arabidopsis thaliana* are mitochondrial transporters of aspartate, glutamate, and dicarboxylates

Received for publication, November 9, 2017, and in revised form, January 15, 2018 Published, Papers in Press, January 25, 2018, DOI 10.1074/jbc.RA117.000771

Magnus Monné[‡§], Lucia Daddabbo[‡], David Gagneul[¶1], Toshihiro Obata[‖], Björn Hielscher[¶2], Luigi Palmieri[‡], Daniela Valeria Miniero[‡], Alisdair R. Fernie[‖3], Andreas P. M. Weber[¶4], and Ferdinando Palmieri[‡**5]**

*From the [‡]Department of Biosciences, Biotechnologies and Biopharmaceutics, Laboratory of Biochemistry and Molecular Biology, University of Bari, via Orabona 4, 70125 Bari, Italy, the [§]Department of Sciences, University of Basilicata, Via Ateneo Lucano 10, 85100 Potenza, Italy, the [¶]Cluster of Excellence on Plant Science (CEPLAS), Institute of Plant Biochemistry, Heinrich-Heine-Universität, Universitätsstrasse 1, 40225 Düsseldorf, Germany, the [‖]Department Willmitzer, Max-Planck-Institut fur Molekulare Pflanzenphysiologie, Am Muhlenberg 1, 14476 Potsdam-Golm, Germany, and the **Center of Excellence in Comparative Genomics, University of Bari, via Orabona 4, 70125 Bari, Italy*

Edited by Joseph M. Jez

The *Arabidopsis thaliana* genome contains 58 members of the solute carrier family SLC25, also called the mitochondrial carrier family, many of which have been shown to transport specific metabolites, nucleotides, and cofactors across the mitochondrial membrane. Here, two *Arabidopsis* members of this family, AtUCP1 and AtUCP2, which were previously thought to be uncoupling proteins and hence named UCP1/PUMP1 and UCP2/PUMP2, respectively, are assigned with a novel function. They were expressed in bacteria, purified, and reconstituted in phospholipid vesicles. Their transport properties demonstrate that they transport amino acids (aspartate, glutamate, cysteine sulfinate, and cysteate), dicarboxylates (malate, oxaloacetate, and 2-oxoglutarate), phosphate, sulfate, and thiosulfate. Transport was saturable and inhibited by mercurials and other mitochondrial carrier inhibitors to various degrees. AtUCP1 and AtUCP2 catalyzed a fast counterexchange transport as well as a low uniport of substrates, with transport rates of AtUCP1 being much higher than those of AtUCP2 in both cases. The aspartate/glutamate heteroexchange mediated by AtUCP1 and AtUCP2 is electroneutral, in contrast to that mediated by the mammalian mitochondrial aspartate glutamate carrier. Furthermore, both carriers were found to be targeted to mitochondria. Metabolite profiling of single and double knockouts shows changes in organic acid and amino acid levels. Notably, AtUCP1 and AtUCP2 are the first reported mitochondrial carriers in *Arabidopsis* to transport aspartate and glutamate. It is proposed that the primary function of AtUCP1 and AtUCP2 is to catalyze an aspartate$_{out}$/glutamate$_{in}$ exchange across the mitochondrial membrane and thereby contribute to the export of reducing equivalents from the mitochondria in photorespiration.

Mitochondrial carriers (MCs)[6] are a large family of membrane proteins that transport nucleotides, amino acids, carboxylic acids, inorganic ions, and cofactors across the mitochondrial inner membrane (1–3). Many metabolic pathways and cellular processes with complete or partial localization in the mitochondrial matrix are dependent on transport steps catalyzed by MCs (*e.g.* oxidative phosphorylation, metabolism of fatty acids and amino acids, gluconeogenesis, thermogenesis, mitochondrial replication, transcription, and translation) (3). The protein sequences of the MC family members have a characteristic three times tandemly repeated 100-residue domain (4), which contains two hydrophobic segments and a signature sequence motif P*X*(D/E)*XX*(K/R)*X*(K/R) (20–30 residues) (D/E)G*XXXX*(W/Y/F)(K/R)G (PROSITE PS50920, PFAM PF00153, and IPR00193) (5). In atomic resolution 3D structures of the only MC family member determined to date (the carboxyatractyloside-inhibited ADP/ATP carrier) (6, 7), the six hydrophobic segments form a bundle of transmembrane α-helices with a central substrate translocation pore, and the three P*X*(D/E)*XX*(K/R) motifs form a gate toward the matrix side. In most cases, the MC signature motif has been used to identify family members in genomic sequences; *Homo sapiens* has 53 members, *Saccharomyces cerevisiae* has 35, and *Arabidopsis thaliana* has 58. About half of these carriers have been identified and characterized in terms of substrate specificity, transport proteins, and kinetic parameters by direct transport assays (1, 8, 9).

This work was supported by grants from the Center of Excellence on Comparative Genomics and Italian Human ProteomeNet Grant RBRN07BMCT_009 (MIUR). The authors declare that they have no conflicts of interest with the contents of this article.

This article contains Tables S1–S4 and Figs. S1–S6.

[1] Present address: Université de Lille, INRA, ISA, Université d' Artois, Université du Littoral Côte d'Opale, EA 7394-ICV-Institut Charles Viollette, F-59000 Lille, France.

[2] Supported by an iGRAD-Plant doctoral fellowship (IRTG 1525).
[3] Work in the laboratory of this author was supported by the Max-Planck-Society.
[4] Supported by the Cluster of Excellence on Plant Science CEPLAS (EXC 1028) and CRC 1208.

[5] To whom correspondence should be addressed: Dept. of Biosciences, Biotechnologies, and Biopharmaceutics, Laboratory of Biochemistry and Molecular Biology, University of Bari, via Orabona 4, 70125 Bari, Italy. Tel.: 39-080-5443323; Fax: 39-080-5442770; E-mail: ferdpalmieri@gmail.com.

[6] The abbreviations used are: MC, mitochondrial carrier; UCP, uncoupling protein; AtUCP1, *A. thaliana* UCP1; AtUCP2, *A. thaliana* UCP2; hUCP2, human UCP2; DIC, dicarboxylate carrier; DTC, di- and tricarboxylate carrier; GDC, glycine decarboxylase; GFP, green fluorescent protein; GS/GOGAT, glutamine synthetase/glutamine oxoglutarate aminotransferase; MAS, malate aspartate shuttle; IVD, isovaleryl-CoA-dehydrogenase; CTD, C-terminal domain.

Transport properties of AtUCP1 and AtUCP2

Studies aiming to biochemically characterize MCs from *A. thaliana* were initiated by comparing selected *Arabidopsis* genes with those of yeast and humans encoding MCs with previously identified substrates (9). *Arabidopsis* has been demonstrated to express MCs for the four main types of substrates (1) (*i.e.* nucleotide carriers for ADP/ATP (AAC1–4, PNC1 and -2, AtBT1, PM-ANT1, and TAAC) (10–16), adenine nucleotides (ADNT1) (17), ATP-Mg/P_i (APC1–3) (18, 19), NAD^+ (NDT1 and -2) (20), NAD^+, NADH, CoA, and adenosine 3′,5′-phosphate (PXN) (21, 22); carboxylate carriers for di- and tricarboxylates (DTC) (23) and dicarboxylates (DIC1–3) (24); amino acid carriers for basic amino acids (BAC1 and -2) (25, 26) and *S*-adenosylmethionine (SAMC1 and -2) (27, 28); and inorganic ion carriers for phosphate and sulfate (29)). It is important to note that some of the carriers characterized from *Arabidopsis* have broader substrate specificities than their human and yeast counterparts, and additionally some of them are localized in compartments other than the mitochondria, such as peroxisomes, chloroplasts, the endoplasmic reticulum, and the plasma membrane (1). It is also noteworthy that the molecular identity of an *Arabidopsis* MC corresponding to the human aspartate/glutamate exchangers (AGC1 and -2) (30) or glutamate uniporters of any type (GC1 and -2) (31) has, to date, not been established.

The mammalian uncoupling protein 1 (UCP1) was demonstrated to transport protons, thereby uncoupling oxidative phosphorylation (32, 33). On the basis of homology with subsequently sequenced MCs, a UCP subfamily was identified containing six members in both humans (hUCP1–6) and *Arabidopsis* (AtUCP1–6). However, AtUCP4–6 were subsequently renamed dicarboxylate carriers (DIC1–3), following the demonstration that they transport malate, oxaloacetate, succinate, P_i, sulfate, thiosulfate, and sulfite (24), and hUCP2 was demonstrated to be a four-carbon metabolite/P_i carrier transporting aspartate, malate, malonate, oxaloacetate, P_i, and sulfate (34).

In the current study, we investigated the potential transport properties of the two closest homologs of hUCP2 in *Arabidopsis*: AtUCP1 and AtUCP2, also known as PUMP1 and PUMP2. Previously, AtUCP1 was shown to be localized to mitochondria and display an uncoupling activity similar to that of hUCP1 (35–37). By contrast, very little is known about AtUCP2; in a proteomic study, it was detected in the Golgi (38), but in another, it was detected at the plasma membrane (39). The results presented here demonstrate that AtUCP1 and the less-studied AtUCP2 are mitochondrially localized isoforms and have a broad substrate specificity, transporting a variety of substrates, including aspartate, glutamate, malate, oxaloacetate, and other metabolites. Characterization of metabolite profiles of T-DNA insertional knockout mutants, including a *ucp1*/*ucp2* double mutant, revealed clear changes in organic acid levels, some of which were exacerbated by the application of salt stress.

Results

Identification of the closest homologs of AtUCP1 and AtUCP2 in various species

The protein sequences of AtUCP1 and AtUCP2 homologs were collected, aligned, and analyzed (Fig. S1). AtUCP1 and AtUCP2 share 72% identical amino acids. Their sequences are much more similar to each other than to any other *Arabidopsis* protein; in *Arabidopsis*, the closest relative to AtUCP1 and AtUCP2 is AtDIC2, which shares 41 and 42% sequence identity with AtUCP1 and AtUCP2, respectively. In humans and *S. cerevisiae*, the closest homologs are hUCP2 (34), having 51 and 44% identical amino acids, and yeast Dic1p (40), exhibiting 30 and 33% sequence identity with AtUCP1 and AtUCP2, respectively. Putative orthologs with high sequence identity with AtUCP1 and AtUCP2 above 75% were found in several plant species. Moreover, from structural sequence alignments using the X-ray structure of the bovine ADP/ATP carrier (6) as a template, it can be deduced that 85 and 54% of the residues lining the surface of the substrate translocation pore are identical between AtUCP1 and AtUCP2 and between AtUCP1, AtUCP2, and hUCP2, respectively. These results suggest that AtUCP1 and AtUCP2 are isoforms, and their closest homolog with identified substrates is hUCP2.

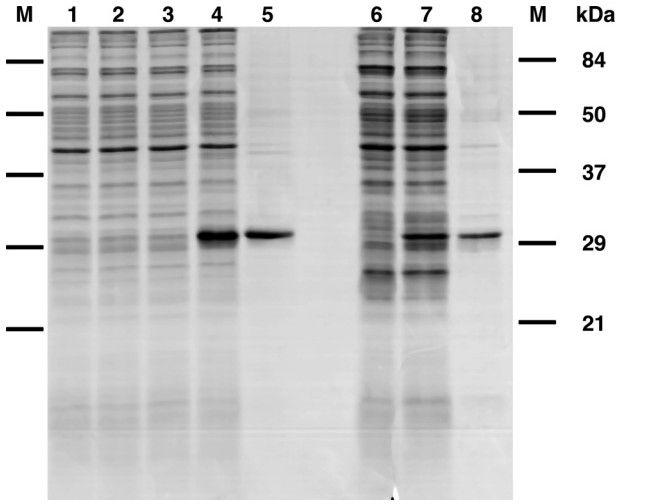

Figure 1. Expression in *Escherichia coli* and purification of AtUCP1 and AtUCP2. Proteins were separated by SDS-PAGE and stained with Coomassie Blue. *Lanes 1–5*, AtUCP1; *lanes 6–8*, AtUCP2. Markers were Bio-Rad prestained SDS-PAGE standards: bovine serum albumin, 84 kDa; ovalbumin, 50 kDa; carbonic anhydrase, 37 kDa; soybean trypsin inhibitor, 29 kDa; lysozyme, 21 kDa). *Lanes 1–4*, *E. coli* BL21(DE3); *lanes 6* and *7*, *E. coli* BL21 CodonPlus(DE3)-RIL containing the expression vector, without (*lanes 1*, *3*, and *6*) and with the coding sequence of AtUCP1 (*lanes 2* and *4*) and the coding sequence of AtUCP2 (*lane 7*). Samples were taken immediately before induction (*lanes 1* and *2*) and 5 h later (*lanes 3*, *4*, *6*, and *7*). The same number of bacteria were analyzed in each sample. *Lanes 5* and *8*, purified AtUCP1 protein (5 μg) and purified AtUCP2 (3 μg) derived from bacteria shown in *lanes 4* and *7*, respectively.

Bacterial expression of AtUCP1 and AtUCP2

AtUCP1 and AtUCP2 were expressed in *Escherichia coli* BL21(DE3) strains (Fig. 1, *lanes 4* and *7*). They accumulated as inclusion bodies and were purified by centrifugation and washing (see "Experimental procedures"). The apparent molecular masses of purified AtUCP1 and AtUCP2 (Fig. 1, *lanes 5* and *8*) were ~31 kDa, which is in good agreement with the calculated value of 33 kDa for both AtUCP1 and AtUCP2. The identities of the recombinant proteins were confirmed by MALDI-TOF mass spectrometry, and the yield of the purified proteins was about 10 and 2 mg/liter of culture for AtUCP1 and AtUCP2, respectively. The proteins were detected neither in non-

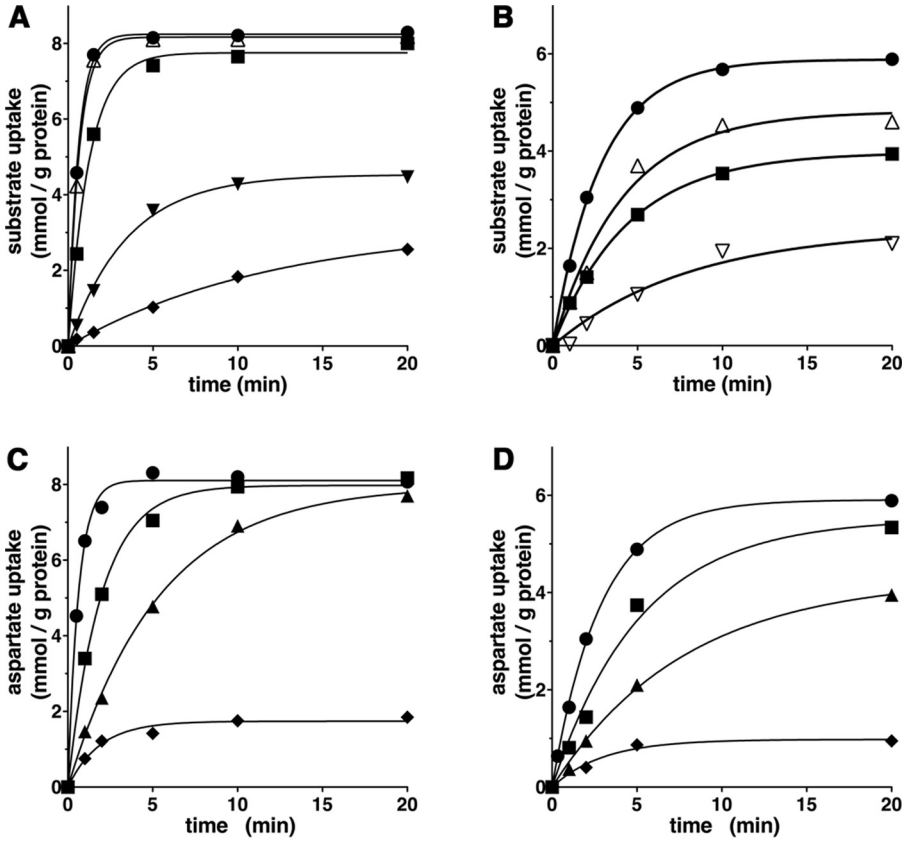

Figure 2. Substrate homo-exchanges in proteoliposomes reconstituted with AtUCP1 (*A* and *C*) and AtUCP2 (*B* and *D*). *A* and *B*, homo-exchanges of aspartate (●), malate (△), glutamate (■), malonate (▼), sulfate (◆), and 2-oxoglutarate (▽) at 25 °C. *C* and *D*, aspartate/aspartate homo-exchange at 4 °C (◆), 8 °C (▲), 16 °C (■), and 25 °C (●). Transport was initiated by adding radioactive substrate (concentration, 1 mM) to proteoliposomes preloaded internally with the same substrate (concentration, 10 mM). The reaction was terminated at the indicated times. Similar results were obtained in at least three independent experiments.

induced cultures nor in cultures with an empty vector (Fig. 1, *lanes 1*, *2*, *3*, and *6*).

Functional characterization of recombinant AtUCP1 and AtUCP2

Recombinant AtUCP1 and AtUCP2 were reconstituted into liposomes, and their transport activities for various radioactive substrates were tested in homo-exchange experiments (*i.e.* with the same external (1 mM) and internal (10 mM) substrate). In a first set of homo-exchange experiments, time-dependent uptake of several radioactive substrates (aspartate, malate, and glutamate for reconstituted AtUCP1 and AtUCP2; malonate and sulfate for AtUCP1; and 2-oxoglutarate for AtUCP2) demonstrated typical curves for carrier-mediated transport (Fig. 2, *A* and *B*). Both AtUCP1- and AtUCP2-mediated homo-exchanges between external [^{14}C]aspartate and internal aspartate were temperature-dependent (Fig. 2, *C* and *D*), as would be expected for protein-catalyzed transport. Furthermore, no [^{14}C]aspartate/aspartate or [^{14}C]malate/malate exchange activity was detected if AtUCP1 and AtUCP2 had been boiled before incorporation into liposomes or if proteoliposomes were reconstituted with lauric acid/sarkosyl-solubilized material from bacterial cells lacking the expression vector for AtUCP1 and AtUCP2 or harvested immediately before induction of expression (data not shown). In all of these experiments, a mixture of pyridoxal-5′-phosphate and bathophenanthroline was used to block the AtUCP1- and AtUCP2-mediated transport reactions at various time points. In addition, AtUCP1 and AtUCP2 were found to catalyze homo-exchanges of glutamate, malonate, malate, succinate, and P_i, whereas no or very low transport was observed with glutamine, arginine, phenylalanine, threonine, valine, proline, γ-aminobutyrate, citrate, ATP, GTP, *S*-adenosylmethionine, or glutathione (Fig. 3).

The substrate specificities of AtUCP1 and AtUCP2 were examined in detail by measuring the initial rate of [^{14}C]aspartate uptake into proteoliposomes that had been preloaded with various potential substrates (Fig. 4). For both AtUCP1 and AtUCP2, the highest activities were observed in the presence of internal aspartate, glutamate, cysteine sulfinate, cysteate, malonate, malate, oxaloacetate, maleate, and (for AtUCP2) 2-oxoglutarate. Both proteins also exchanged, albeit to a lower extent, internal D-aspartate, cysteine, oxalate, succinate, 2-oxoglutarate, α-aminoadipate, P_i, sulfate, and thiosulfate. In addition, AtUCP2 exchanged [^{14}C]aspartate with the internal substrates (Fig. 4*B*) fumarate, glutarate, and nitrate, which were not significantly transported by AtUCP1 (Fig. 4*A*). By contrast, the uptake of labeled aspartate by AtUCP1 and AtUCP2 was negligible with internal asparagine, D-glutamate, glutamine, serine, glycine, homocysteate, adipate, α-ketoadipate, pyrophosphate, citrate, pyruvate, lactate, phosphoenolpyruvate, acetoacetate, β-hydroxybutyrate, *N*-acetylaspartate, ATP, and

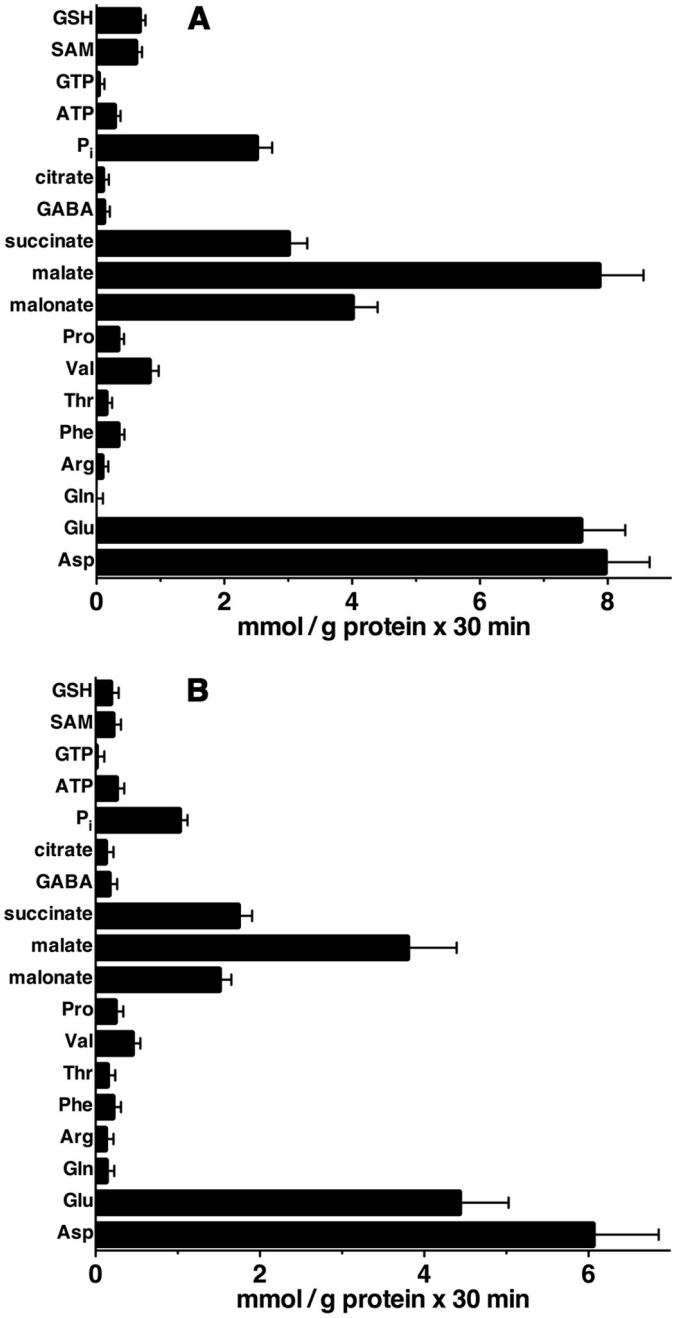

Figure 3. AtUCP1- and AtUCP2-mediated homo-exchanges of various substrates. Proteoliposomes reconstituted with AtUCP1 (*A*) and AtUCP2 (*B*) were preloaded internally with the substrates indicated in the figure (concentration, 10 mM). Transport was initiated by adding radioactive substrate (concentration, 1 mM) to proteoliposomes containing the same substrate. The reaction was terminated after 30 min. The values are means ± S.E. (*error bars*) of at least three independent experiments. *SAM*, *S*-adenosylmethionine.

glutathione (Fig. 4, *A* and *B*). The activity in the presence of these substrates was approximately the same as that observed in the presence of NaCl and no substrate.

The effects of other mitochondrial carrier inhibitors on the [^{14}C]aspartate/aspartate exchange reaction catalyzed by reconstituted AtUCP1 and AtUCP2 were also examined. This transport activity was inhibited strongly by bathophenanthroline, pyridoxal-5′-phosphate, and tannic acid and markedly by mersalyl, $HgCl_2$, and butylmalonate (Fig. 5). Phenylsuccinate and *p*-hydroxymercuribenzoate strongly inhibited AtUCP1 and partially inhibited AtUCP2, whereas bromcresol purple and α-cyano-4-hydroxycinnamate caused partial inhibition of both carriers. By contrast, carboxyatractyloside, bongkrekic acid, and *N*-ethylmaleimide had little or no effect on either AtUCP1 or AtUCP2 activity.

Kinetic characteristics of recombinant AtUCP1 and AtUCP2 proteins

In Fig. 6, the kinetics of 1 mM [^{14}C]aspartate (*A* and *B*) or 1 mM [^{14}C]malate (*C* and *D*) uptake into proteoliposomes catalyzed by recombinant AtUCP1 (*A* and *C*) or AtUCP2 (*B* and *D*) and measured either as uniport (with internal NaCl) or as exchange (in the presence of 10 mM substrates) are compared. The [^{14}C]aspartate/aspartate and [^{14}C]malate/malate exchanges followed first-order kinetics (rate constants 1.6 and 1.4 min^{-1} (AtUCP1) or 0.27 and 0.23 min^{-1} (AtUCP2); initial rates 14 and 11 mmol/min × g of protein (AtUCP1) or 1.9 and 1.3 mmol/min × g of protein (AtUCP2), respectively), isotopic equilibrium being approached exponentially. By contrast, with internal NaCl and no substrate, very low uptake of [^{14}C]aspartate or [^{14}C]malate was observed by liposomes reconstituted either with AtUCP1 or AtUCP2, suggesting that the two proteins catalyze a minor unidirectional transport (uniport) of substrates. In addition, Fig. 6 (*A–D*) illustrates the time courses of several AtUCP1-mediated and AtUCP2-mediated hetero-exchanges between [^{14}C]aspartate or [^{14}C]malate and other transported substrates. The data of Fig. 6 (*A* and *C*) show that AtUCP1 transports cysteate much better than D-aspartate and dicarboxylates with the following order of efficiency: malate > oxaloacetate > malonate > succinate (these substrates better than P_i). Similarly, the data of Fig. 6 (*B* and *D*) demonstrate that cysteate is transported slightly better than D-aspartate and malate more efficiently than oxaloacetate by AtUCP2. The uniport mode of transport was further investigated by measuring the efflux of [^{14}C]aspartate or [^{14}C]malate from preloaded active proteoliposomes because it provides a more convenient assay for unidirectional transport (41). In the absence of external substrate, significant efflux of [^{14}C]aspartate (Fig. 7, *A* and *B*) or [^{14}C]malate (Fig. 7, *C* and *D*) catalyzed by both AtUCP1 and AtUCP2 was observed. However, in the presence of external substrates, the efflux transport rates were at least one order of magnitude higher. These experiments demonstrate that AtUCP1 and AtUCP2 are capable of catalyzing both a rapid antiport of substrates and a slow uniport transport.

The kinetic constants of AtUCP1 and AtUCP2 were determined from the initial transport rates of homo-exchanges at various external labeled substrate concentrations in the presence of a constant saturating internal substrate concentration. The Michaelis constants (K_m) of the two recombinant proteins for aspartate were about 0.8 mM, and for glutamate and malate, they were between 1.9 and 2.5 mM. The maximal activities (V_{max}) for aspartate, glutamate, and malate varied between 24 and 33 mmol/min × g of protein for AtUCP1 and 4.2 and 4.5 mmol/min × g of protein for AtUCP2 (Table 1). Glutamate, malate, cysteine sulfinate, cysteate, oxaloacetate, α-ketoglutarate, and sulfate were competitive inhibitors of the AtUCP1- and AtUCP2-mediated [^{14}C]aspartate/aspartate exchanges, as

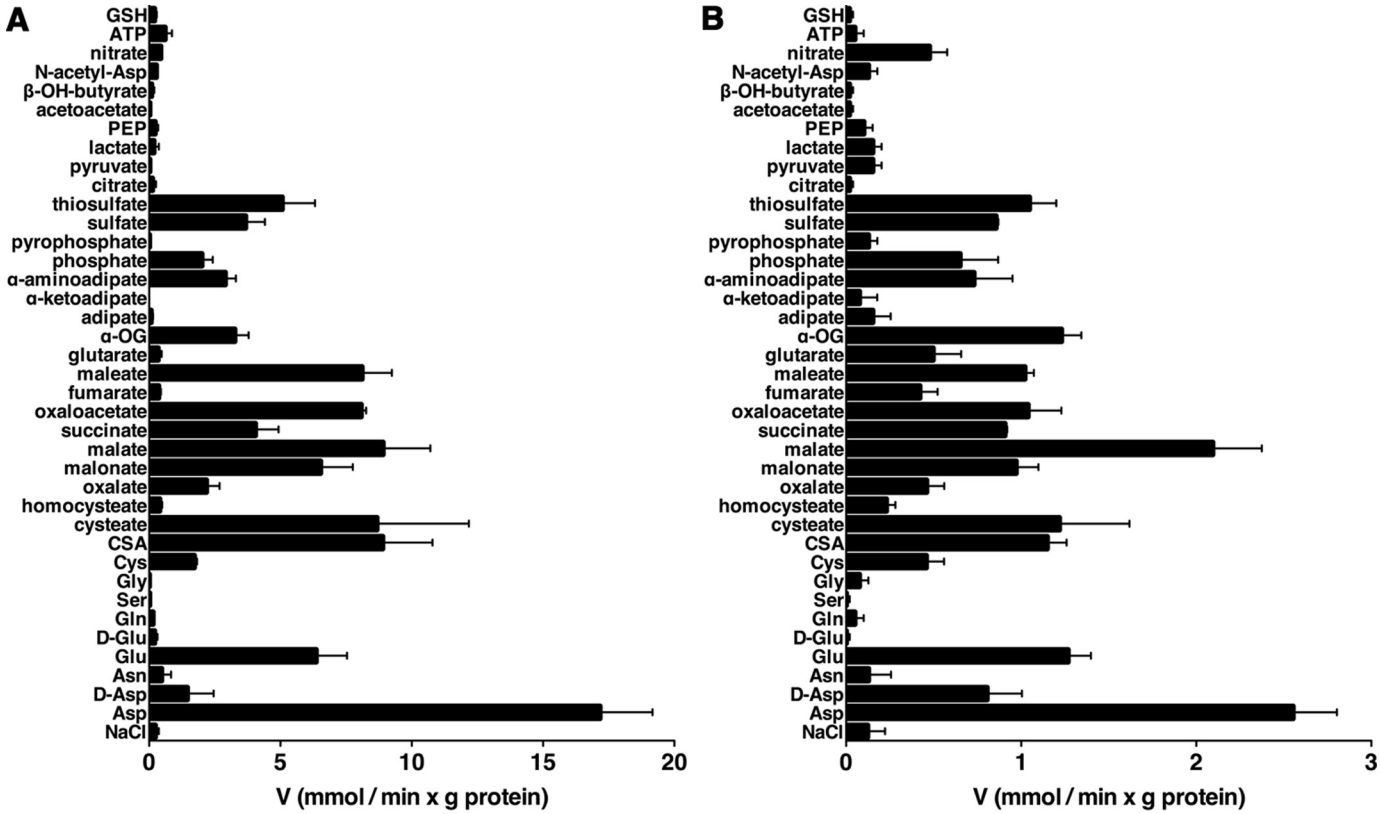

Figure 4. Substrate specificity of AtUCP1 and AtUCP2. Proteoliposomes were preloaded internally with various substrates (concentration, 10 mM). Transport was started by adding 0.8 mM [^{14}C]aspartate and stopped after 7 and 20 s for AtUCP1 (*A*) and AtUCP2 (*B*), respectively. The values are means ± S.E. (*error bars*) of at least three independent experiments. α-*OG*, α-ketoglutarate; *CSA*, cysteinesulfinic acid; *PEP*, phosphoenolpyruvate.

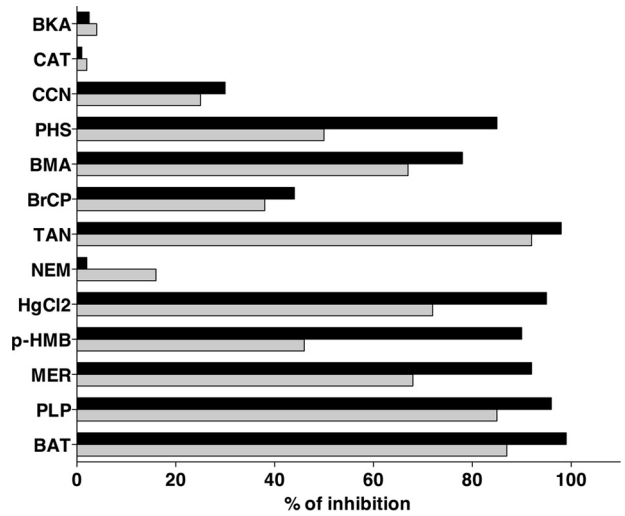

Figure 5. Effect of mitochondrial carrier inhibitors on the rate of AtUCP1- and AtUCP2-mediated [^{14}C]aspartate/aspartate exchange. Proteoliposomes were preloaded internally with 10 mM aspartate, and transport was initiated by adding 1 mM [^{14}C]aspartate. The incubation time was 7 and 20 s for AtUCP1 and AtUCP2, respectively. Thiol reagents and α-cyanocinnamate were added 2 min before the labeled substrate; the other inhibitors were added together with [^{14}C]aspartate. The final concentrations of the inhibitors were as follows: 10 μM for mercuric chloride ($HgCl_2$), carboxyatractyloside (*CAT*), and bongkrekic acid (*BKA*); 0.1 mM for mersalyl (*MER*) and *p*-hydroxymercuribenzoate (*pHMB*); 0.2 mM for bromcresol purple (*BrCP*); 1 mM for *N*-ethylmaleimide (*NEM*) and α-cyanocinnamate (*CCN*); 5 mM for butylmalonate (BMA) and phenylsuccinate (*PHS*); 25 mM for bathophenanthroline (*BAT*); 30 mM for pyridoxal 5′-phosphate (*PLP*); and 0.2% for tannic acid (*TAN*). The extents of inhibition (percentages) for AtUCP1 (*black bars*) and AtUCP2 (*gray bars*) from a representative experiment are given. Similar results were obtained in at least three independent experiments.

they increased the apparent K_m without changing the V_{max} (not shown). The inhibition constants (K_i) of these compounds are listed in Table 2.

Influence of membrane potential and pH gradient on the AtUCP1- and AtUCP2-mediated exchange reactions

Given that the mammalian aspartate glutamate carriers AGC1 and -2 have been shown to catalyze an electrophoretic exchange between aspartate$^-$ and glutamate$^-$ + H^+ (30), we investigated the influence of the membrane potential on the [^{14}C]aspartate/glutamate exchange catalyzed by recombinant AtUCP1 and AtUCP2. A K^+-diffusion potential was generated across the proteoliposomal membranes with valinomycin in the presence of a K^+ gradient of 1:50 (mM/mM, in/out), corresponding to a calculated value of about 100 mV positive inside (Table 3). The rate of the [^{14}C]aspartate$_{out}$/glutamate$_{in}$ heteroexchange was unaffected by valinomycin in the presence of the K^+ gradient. By contrast, the aspartate$_{out}$/glutamate$_{in}$ exchange, mediated by recombinant AGC2 C-terminal domain (AGC2-CTD) (30), was stimulated under the same experimental conditions. These results indicate that the AtUCP1- and AtUCP2-mediated aspartate/glutamate hetero-exchange is not electrophoretic but electroneutral, suggesting that AtUCP1 and AtUCP2 transport either aspartate$^-$ for glutamate$^-$ or both together with a H^+. Also, the AtUCP1- and AtUCP2-mediated aspartate/aspartate, malate/malate, and malate$_{out}$/aspartate$_{in}$ (Table 3) and malate$_{out}$/glutamate$_{in}$ (data not shown) were unaffected by valinomycin in the presence of a K^+ gradient of 1:50. In view of the different charges carried by the amino

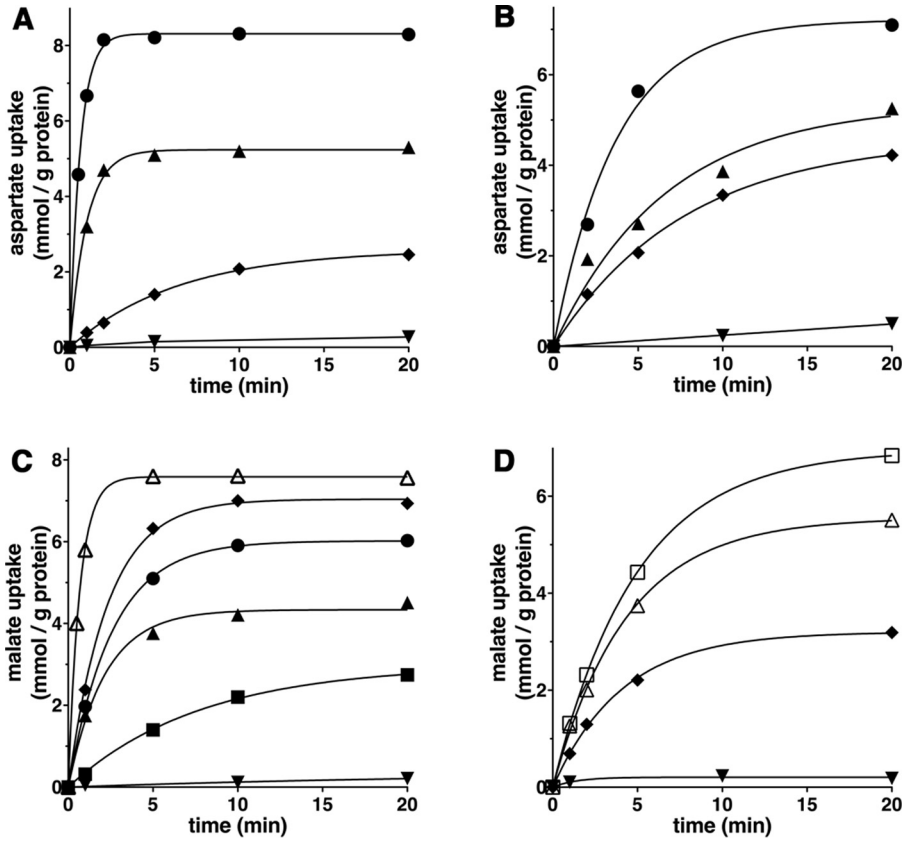

Figure 6. Kinetics of [^{14}C]aspartate or [^{14}C]malate uptake by AtUCP1- and AtUCP2-reconstituted liposomes containing no substrate or various substrates. Proteoliposomes containing AtUCP1 (*A* and *C*) or AtUCP2 (*B* and *D*) were preloaded internally with 10 mM aspartate (●), cysteate (▲), D-aspartate (◆), or 10 mM NaCl and no substrate (▼) (*A* and *B*) and with malate (△), oxaloacetate (◆), malonate (●), succinate (▲), phosphate (■), aspartate (□), or 10 mM NaCl and no substrate (▼) (*C* and *D*). Transport was initiated by adding 1 mM [^{14}C]aspartate (*A* and *B*) or 1 mM [^{14}C]malate (*C* and *D*) and terminated at the indicated times. Similar results were obtained in at least three independent experiments.

acids aspartate and glutamate and dicarboxylates at physiological pH levels, we explored whether the charge imbalance of the malate/aspartate and malate/glutamate hetero-exchanges catalyzed by AtUCP1 and AtUCP2 is compensated by proton movement. A pH difference across the liposomal membranes (basic inside the vesicles) was created by the addition of the K^+/H^+ exchanger nigericin to proteoliposomes in the presence of a K^+ gradient of 1:50 (mM/mM, in/out). Under these conditions, the uptake of [^{14}C]malate in exchange for internal aspartate or glutamate increased (Table 3), whereas the uptake of [^{14}C]malate in exchange for internal malate or 2-oxoglutarate was unaffected (data not shown). Therefore, the charge imbalance of the substrates exchanged by AtUCP1 and AtUCP2 is compensated by the movement of protons.

Subcellular localization of AtUCP1 and AtUCP2 proteins in transiently transformed Nicotiana benthamiana leaf cells

C-terminal fusion proteins of AtUCP1 and AtUCP2 with the green fluorescent protein (GFP) under the control of an *Arabidopsis* ubiquitin-10 promoter were transiently expressed in *N. benthamiana* to investigate the subcellular localization via confocal laser-scanning microscopy. Simultaneously, *N. benthamiana* was co-infiltrated with the mitochondrion-located *Arabidopsis* isovaleryl-CoA-dehydrogenase tagged with a C-terminal eqFP611 (IVD-eqFP611) under the control of the cauliflower mosaic virus 35S promoter. Two days after infiltration, protoplasts were isolated from leaf tissue and directly used for microscopy.

The C-terminal fusion proteins AtUCP1-GFP (Fig. 8*A*) and AtUCP2-GFP (Fig. 8*B*) (shown in *green*) clearly overlap with almost all mitochondrial IVD-eqFP611 fluorescent signals (shown in *red*) in all observed protoplasts, indicating the mitochondrial localization of both proteins. 48 h after infiltration, the mitochondrial marker was generally higher-expressed than the GFP fusion proteins and was also found in the cytosol with more prominent fluorescent signals detected in mitochondria.

Isolation, generation, and metabolic characterization of AtUCP1–2 knockout mutants

After biochemically characterizing the properties of recombinant AtUCP1 and AtUCP2 proteins, we turned our attention to evaluating their physiological role in *Arabidopsis*. For this purpose, we acquired the individual T-DNA insertion mutants and crossed them to obtain the *ucp1*/*ucp2* double mutant (Fig. S2). The *ucp1* line used here was extensively characterized by Sweetlove *et al.* (37), including functional complementation by the *UCP1* genomic sequence. This mutant harbors a T-DNA insertion in the first intron and shows low residual UPC protein amounts in the mitochondria (5% of the wildtype line (37)). Congruent with this previous work, we also detected residual expression of the *UCP1* gene, which was much lower than that of the wildtype (Fig. S3). The expression of the *UCP2* gene was

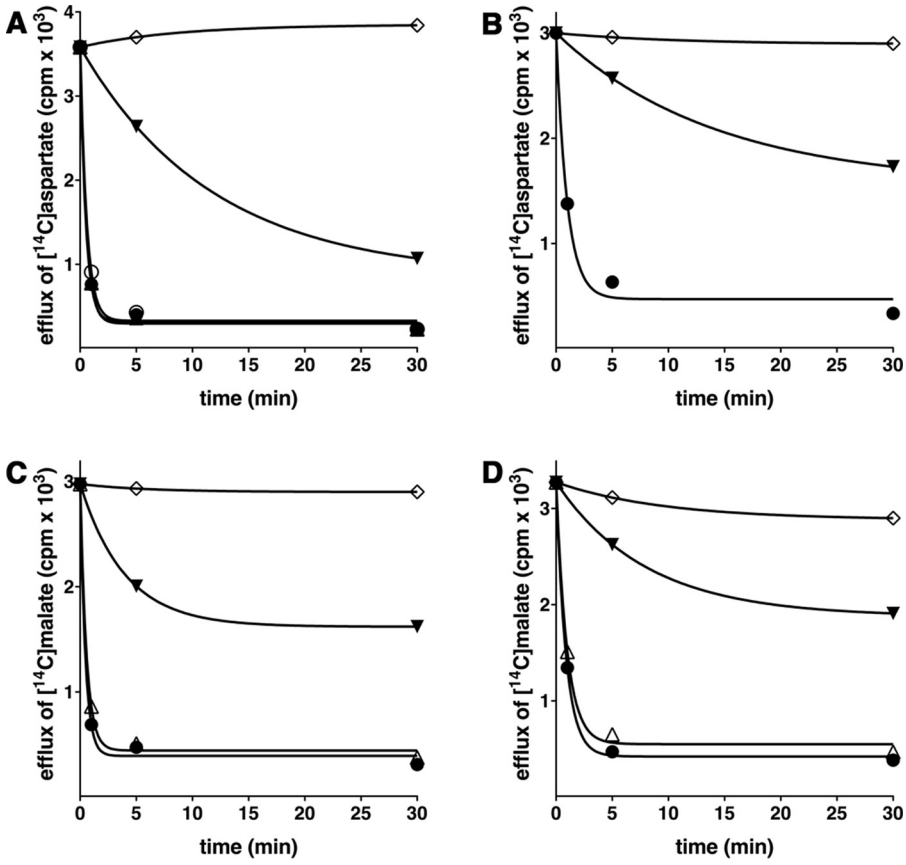

Figure 7. Efflux of [^{14}C]aspartate and [^{14}C]malate from AtUCP1- and AtUCP2-reconstituted liposomes. Proteoliposomes containing AtUCP1 (*A* and *C*) and AtUCP2 (*B* and *D*) with 5 mM aspartate and 5 mM malate internally were loaded with [^{14}C]aspartate and [^{14}C]malate, respectively, by carrier-mediated exchange equilibrium, and external substrate was removed by Sephadex G-75. Efflux of [^{14}C]aspartate (*A* and *B*) and [^{14}C]malate (*C* and *D*) was started by adding 5 mM aspartate (●), malate (△), glutamate (○), 5 mM NaCl and no substrate (▼), and 5 mM aspartate (*A* and *B*) or 5 mM malate (*C* and *D*) together with 20 mM pyridoxal 5′-phosphate and 20 mM bathophenanthroline (◇). The transport was terminated at the indicated times. Similar results were obtained in at least three independent experiments.

Table 1

Kinetic constants of recombinant AtUCP1 and AtUCP2

The values were calculated from linear regression of double reciprocal plots of the initial rates of the indicated homo-exchanges *versus* the external substrate concentration. The exchanges were started by adding appropriate concentrations of labeled substrate to proteoliposomes preloaded internally with the same substrate (10 mM). The reaction time was 7 and 20 s for AtUCP1 and AtUCP2, respectively. The values are means ± S.E. of at least three independent experiments carried out in duplicate.

Carrier and substrate	K_m	V_{max}
	mM	*mmol/min × g protein*
AtUCP1		
[^{14}C]Aspartate/aspartate	0.8 ± 0.1	30 ± 6
[^{14}C]Glutamate/glutamate	1.9 ± 0.2	24 ± 6
[^{14}C]Malate/malate	2.0 ± 0.2	33 ± 6
AtUCP2		
[^{14}C]Aspartate/aspartate	0.8 ± 0.1	4.5 ± 0.5
[^{14}C]Glutamate/glutamate	2.5 ± 0.2	4.2 ± 0.4
[^{14}C]Malate/malate	2.4 ± 0.1	4.3 ± 0.4

Table 2

Competitive inhibition by various substrates of [^{14}C]aspartate uptake into proteoliposomes reconstituted with AtUCP1 or AtUCP2

The inhibition constants (K_i) were calculated from Dixon plots of the inverse rate of [^{14}C]aspartate transport *versus* the competing substrate concentration. The competing substrates at appropriate concentrations were added together with labeled asparate to proteoliposomes containing 10 mM aspartate. The values are means ± S.E. of at least three independent experiments carried out in duplicate.

Inhibitor	K_i	
	AtUCP1	AtUCP2
	mM	
α-Ketoglutarate	3.3 ± 0.2	2.6 ± 0.2
Cysteate	2.2 ± 0.3	2.4 ± 0.2
Cysteinesulfinate	2.7 ± 0.3	2.3 ± 0.2
Glutamate	2.2 ± 0.2	2.3 ± 0.2
Malate	1.7 ± 0.2	2.2 ± 0.2
Oxaloacetate	2.6 ± 0.3	3.2 ± 0.2
Sulfate	3.6 ± 0.3	3.3 ± 0.3

virtually absent in the newly isolated *ucp2* mutant (Fig. S3). Having these genotypes in hand, we next assessed their metabolic phenotypes via GC-MS–based metabolic profiling both in plants grown on normal MS agar and in plants exposed to salt stress. The effects of salt stress were investigated because UCPs have been previously proposed to contribute to the abiotic stress response (36). The clearest metabolic phenotype was that observed in the organic acids; however, changes in phenylalanine, serine, the branched chain amino acids, ornithine, *myo*-inositol, putrescine, and AMP were apparent in one or more of the genotypes (Fig. 9 and Tables S1–S3). These metabolite profiles are thus consistent with the transport assay data suggesting that AtUCP1 and AtUCP2 are important in organic and amino acid metabolism in plants. The metabolic phenotypes of the *ucp1*/*ucp2* double mutant tend to be similar to those of *ucp1*, suggesting a predominant role of UCP1 in *Arabidopsis*, at least in the leaf tissue assayed in the work reported here. Regarding the observed changes, interestingly, for the levels of some of the metabolites, such as malate and fumarate, the imposition of salt stress exacerbated intergenotypic differences. For others, such

Table 3

Influence of membrane potential and pH gradient on the activity of reconstituted AtUCP1 and AtUCP2

The exchanges were started by adding 0.8 mM [^{14}C]aspartate or 0.8 mM [^{14}C]malate to AtUCP1- and AtUCP2-reconstituted proteoliposomes. For the measurements of the aspartate/glutamate carrier activity, 50 μM [^{14}C]aspartate was added to proteoliposomes reconstituted with AGC2-CTD. K^+_{in} was in included as KCl in the reconstitution mixture, whereas K^+_{out} was added as KCl together with the labeled substrate. Valinomycin or nigericin was added in 10 μl ethanol/ml of proteoliposomes, whereas the control samples contained the solvent alone. 20 mM or 2 mM PIPES (pH 7.0) was present inside and outside the proteoliposomes in the experiments with valinomycin or nigericin, respectively. The exchange reactions were stopped after 7, 20, and 30 s for AtUCP1, AtUCP2, and AGC2-CTD, respectively. The values are means ± S.E. of four independent experiments carried out in duplicate.

Uptake of	Internal substrate	K^+_{in}/ K^+_{out}	Transport activity (mmol / min x g protein)					
			AtUCP1		AtUCP2		AGC2-CTD	
			Control	Valinomycin	Control	Valinomycin	Control	Valinomycin
[^{14}C]aspartate	aspartate	1/1	16 ± 2	16 ± 2	2.5 ± 0.4	2.7 ± 0.3	0.19 ± 0.03	0.22 ± 0.02
		1/50	16 ± 2	16 ± 2	2.6 ± 0.3	2.4 ± 0.4	0.20 ± 0.03	0.20 ± 0.04
	glutamate	1/1	6 ± 1	6 ± 1	1.2 ± 0.2	1.3 ± 0.2	0.16 ± 0.03	0.13 ± 0.02
		1/50	7 ± 1	6 ± 1	1.0 ± 0.2	1.2 ± 0.3	0.14 ± 0.02	0.42 ± 0.05
[^{14}C]malate	malate	1/1	10 ± 1	9 ± 1	1.0 ± 0.2	1.1 ± 0.2		
		1/50	10 ± 1	10 ± 1	0.9 ± 0.2	1.1 ± 0.3		
	aspartate	1/1	12 ± 1	12 ± 2	1.1 ± 0.2	1.3 ± 0.2		
		1/50	11 ± 1	11 ± 2	1.3 ± 0.2	1.2 ± 0.2		
			Control	Nigericin	Control	Nigericin		
[^{14}C]malate	aspartate	1/1	9 ± 1	9 ± 1	2.6 ± 0.3	2.1 ± 0.2		
		1/50	9 ± 1	18 ± 1	2.5 ± 0.2	4.2 ± 0.3		
	glutamate	1/1	8 ± 1	7 ± 1	1.5 ± 0.3	1.7 ± 0.2		
		1/50	8 ± 1	19 ± 1	1.8 ± 0.2	3.0 ± 0.2		

as citrate, these differences were ameliorated (Fig. 9). The complexity of these results suggests that further research is warranted into the precise physiological role(s) of these proteins under both optimal and suboptimal conditions and in different plant tissues and developmental stages.

Discussion

A recent report has shown that the MC family member hUCP2, which was thought to have a UCP1-like uncoupling activity (42, 43), transports aspartate, 4-carbon dicarboxylates, phosphate, and sulfate (34). The percentages of identical amino acids between hUCP2 and AtUCP1 (51%) and AtUCP2 (44%) suggest that these proteins are highly related to one another. However, it is not possible to make reliable assumptions about the substrate specificity or about the transport modes on the basis of the amino acid similarity, given that even close MC homologs, such as isoforms 1 and 2 of the human ornithine carrier having 87% identical sequences, exhibit considerable differences in substrate specificity and transport kinetics (44, 45). Therefore, we decided to investigate the transport properties of AtUCP1 and AtUCP2 by recombinant expression, purification, and reconstitution into liposomes (the EPRA method (9)).

The results presented in this study demonstrate that AtUCP1 and AtUCP2 both transport aspartate, glutamate, cysteine sulfinate, cysteate, malonate, malate, oxaloacetate, and 2-oxoglutarate and, to a lesser extent, D-aspartate, cysteine, oxalate, succinate, P_i, sulfate, and thiosulfate (Fig. 4). In addition, AtUCP2 also transports fumarate, glutarate, and nitrate to some extent (Fig. 4*B*). The substrate specificities of AtUCP1 and AtUCP2 are, therefore, (i) similar as expected in light of their high sequence identity (72%) and (ii) broader than those of previously characterized mitochondrial carriers (9), given that their substrates overlap those of hUCP2 and those of the aspar-

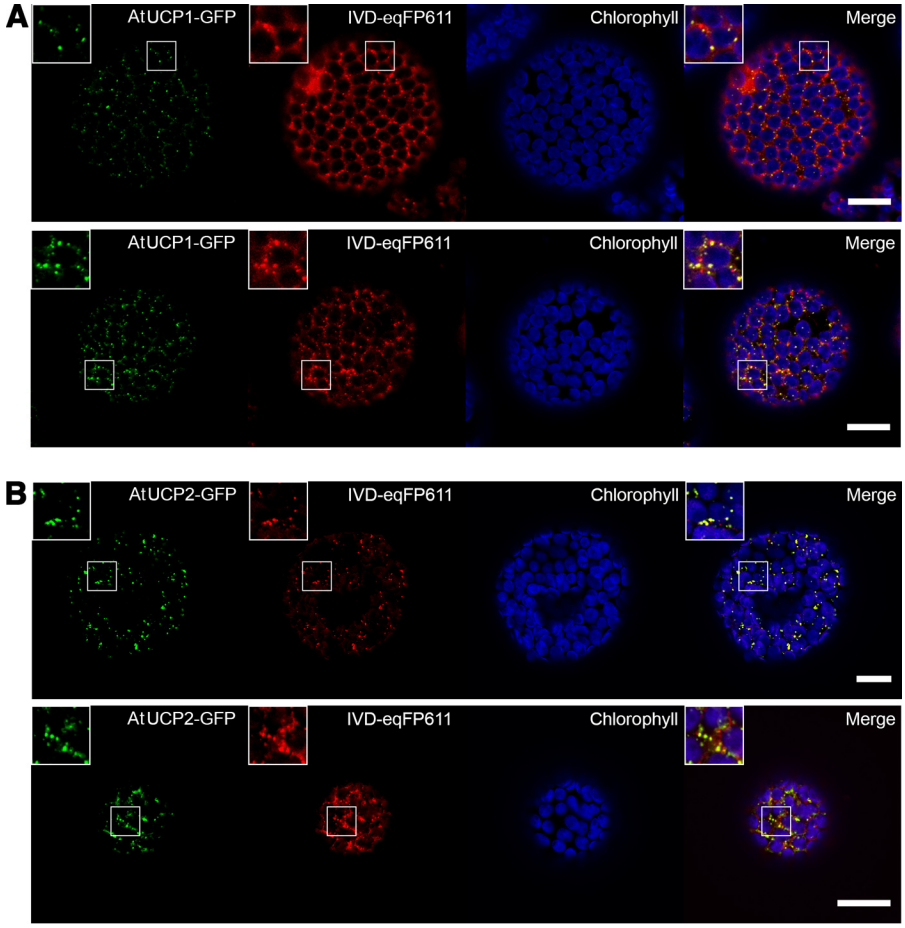

Figure 8. Subcellular localization of AtUCP1-/AtUCP2-GFP fusion proteins in *N. benthamiana* protoplasts. Fluorescent signals of AtUCP1-/AtUCP2-GFP (*green*), mitochondrial marker IVD-eqFP611 (*red*), chlorophyll A/chloroplasts (*blue*), and merge showing the overlap of the fluorescent signals (*yellow*) detected via confocal laser-scanning microscopy. *A*, co-localization of AtUCP1-GFP with the mitochondrial marker. *B*, co-localization of AtUCP2-GFP with the mitochondrial marker. *Scale bar*, 20 μM. Two independently transformed cells are shown in each *panel*.

tate/glutamate and dicarboxylate carriers (24, 30, 40, 46, 47). AtUCP1 and AtUCP2 share a number of similar transport properties; for example, both proteins catalyze a highly efficient counterexchange of substrates; do not transport mono- and tricarboxylates, nucleotides, and other amino acids; respond similarly to the inhibitors tested; and have similar transport affinities (K_i) for aspartate, glutamate, and malate. However, they greatly differ for their specific activities (V_{max}), AtUCP1 being much more active than AtUCP2, although both activities are similar or higher than those exhibited by most mitochondrial carriers characterized to date (1, 9). Furthermore, some substrates (*e.g.* D-aspartate and 2-oxoglutarate) are transported at higher rates by AtUCP2 than AtUCP1 compared with the respective [^{14}C]aspartate/aspartate exchanges.

The results of recombinant protein studies are largely consistent with the *in vivo* evaluation of the function of the proteins that was possible via the isolation and crossing of the respective knockout mutants. Thus, the metabolic phenotype of the mutants was characterized by changes in organic acid and amino acid levels, which are probably due to altered exchanges of these metabolites between the mitochondria and cytosol. However, the differences in metabolite content of the knockouts, which were dependent on salt stress, are difficult to disentangle, and this will probably require considerable further research effort.

Two additional remarks regarding the transport properties of AtUCP1 and AtUCP2 should be made. First, the close biochemical similarities between AtUCP1 and AtUCP2 are understandable, given the commonality of their gene structures; both genes (At3g54110 and At5g58970) share an identical exon/intron structure. We therefore assume that they derive from a common molecular ancestor, accounting for their similarities in biochemical properties. After gene duplication, independent evolution took place allowing the development of individual properties, such as the different specific activity and slightly different substrate preference. Second, our transport measurements, in agreement with the previous data on AtUCP3–6 (24) and hUCP2 (34), are in contrast with the idea that AtUCP1–6 as well as the human UCP1–6 are all "uncoupling proteins" transporting protons and dissipating the proton motive force generated by the respiratory chain. In particular, our findings show that AtUCP1 and AtUCP2 greatly differ from AtUCP4–6 (previously demonstrated to be dicarboxylate carriers) and suggest that they also differ from AtUCP3, which displays only 35 and 37% identical amino acids with AtUCP1 and AtUCP2, respectively. Several protein sequences available in databases

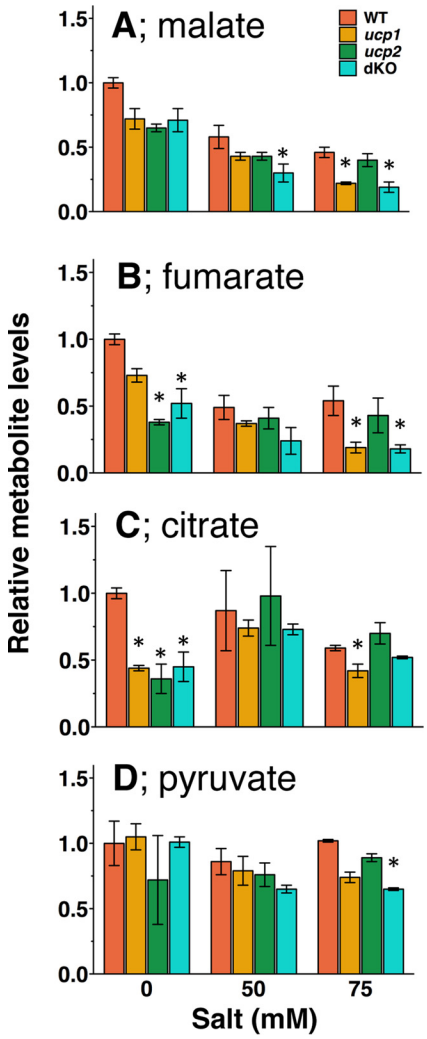

Figure 9. Levels of organic acids in the seedlings of AtUCP knockouts exposed or not to salt stress. Plants were grown on the plates containing 0, 50, and 75 mM NaCl for 12 days, and the relative levels of malate (*A*), fumarate (*B*), citrate (*C*), and pyruvate (*D*) in whole seedlings were determined. The levels of the metabolites were normalized to the mean of those of wildtype plants grown on the plate without salt. The means ± S.E. (*error bars*) from plants grown on three individual plates are shown. *Orange*, wildtype; *brown*, *ucp1*; *green*, *ucp2*; *light green*, *ucp1/ucp2* double knockout.

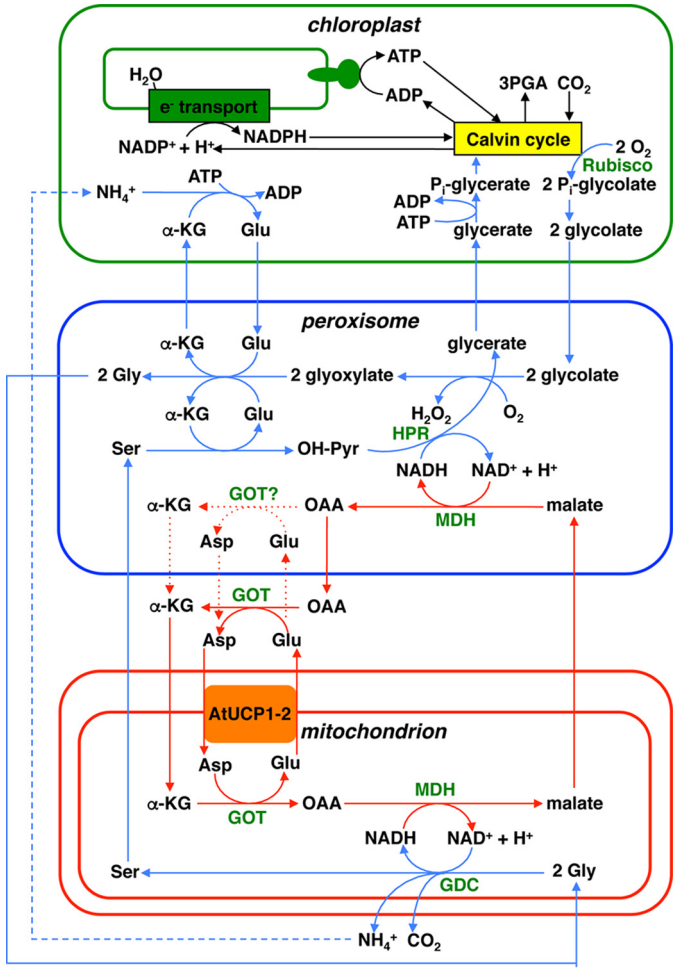

Figure 10. Role of AtUCP1 and AtUCP2 in photorespiration. *Blue* and *red lines* with *arrows* indicate the flow of the glycolate pathway and the transport of reducing equivalents, respectively. *Blue* and *red dashed lines* with *arrows* indicate several transformation steps and alternative paths, respectively. The presence of GOT in the peroxisomes, which is uncertain, has been drawn. Compounds are abbreviated in *black* as follows. α-*KG*, α-ketoglutarate; *OAA*, oxaloacetate; *OH-Pyr*, hydroxypyruvate. Enzymes are abbreviated in *green*. *GDC*, glycine decarboxylate; *GOT*, glutamate oxaloacetate transaminase; *HPR*, hydroxypyruvate reductase; *MDH*, malate dehydrogenase. The figure is modified from Refs. 37 and 51.

are likely to be orthologs of AtUCP1 and AtUCP2 in monocots, dicots, conifers, mosses, and green algae species. These sequences include A9PAU0_POPTR and B9GIV8_POPTR from *Populus trichocarpa* (86 and 79% identity with AtUCP1 and AtUCP2, respectively), A0A077DCK6_TOBAC from *Nicotiana tabacum* (84% identity with AtUCP1), C6T891_SOYBN from *Glycine max* (84% identity), I3ST66_LOTJA from *Lotus japonicus* (83% identity), A9RLI6_PHYP from *Physcomitrella patens* (81% identity), A9P0D2_PICSI from *Picea sitchensis* (79% identity), Q2QZ12_ORYSJ from *Oryza sativa* (77% identity), Q8S4C4_MAIZE from *Zea mays* (76% identity), and A8J1X0_CHLRE from *Chlamydomonas reinhardtii* (76% identity) (Fig. S1). To our knowledge, none of these proteins have been characterized biochemically.

Previous analyses of AtUCP1 knockout mutants revealed impaired photorespiration due to a dramatic decrease in mitochondrial glycine oxidation rate, which led to the suggestion of a physiological role of AtUCP1 in uncoupling the mitochondrial membrane potential for fine-tuning the cell redox state concomitant with photorespiration (37). The substrate specificity and high transport activity of AtUCP1 revealed in this study shed new light on its role in photorespiration. We suggest that AtUCP1 is involved in the glycolate pathway by playing a role in the transfer of reducing equivalents across the mitochondrial inner membrane (Fig. 10). In the glycolate pathway, 2-phosphoglycolate formed from O_2 usage by Rubisco in chloroplasts needs to be transformed in a series of reactions localized in peroxisomes and mitochondria in order to return to the Calvin–Benson cycle as 3-phosphoglycerate. The mitochondrial reaction catalyzed by glycine decarboxylase (GDC), which is the most abundant enzyme in plant mitochondria, reduces NAD^+ to NADH, and peroxisomal hydroxypyruvate reductase oxidizes NADH to NAD^+. This implies that the reducing equivalents of NADH are transported from the mitochondria to the peroxisomes as malate (Fig. 10). In this respect, AtUCP1 (and AtUCP2) would mainly transport aspartate and glutamate

as components of the mitochondrial malate/aspartate shuttle (MAS), which has been suggested to exist in plants in connection to photorespiration (48, 49). More precisely, we propose that the primary function of AtUCP1 (and AtUCP2) is to catalyze an exchange of aspartate$_{out}$ for glutamate$_{in}$ across the inner mitochondrial membrane, thus contributing to the export of reducing equivalents of NADH from mitochondria in conjunction with the other enzymes of MAS. In mammals, MAS transfers the reducing equivalents of NADH from the cytosol to the mitochondria (*i.e.* in the opposite direction of that occurring during photorespiration) because the aspartate glutamate carriers (AGC1 and -2) catalyze an electrophoretic exchange of aspartate$^-$ for glutamate$^-$ + H^+, and hence exit of aspartate and entry of glutamate are greatly favored in active mitochondria with a positive membrane potential outside, making the aspartate/glutamate exchange and the entire MAS unidirectional. By striking contrast, the aspartate/glutamate exchanges mediated by AtUCP1 and AtUCP2 are electroneutral (Table 3) and therefore independent from the proton motive force existing across the mitochondrial membrane. The hypothesis that AtUCP1 and AtUCP2 are involved in the glycolate pathway by catalyzing an aspartate$_{out}$/glutamate$_{in}$ exchange and thereby contributing to the export of reducing equivalents from the mitochondrial matrix is supported by the following considerations: (i) aspartate and glutamate, to the best of our knowledge, are only transported by AtUCP1 (and AtUCP2) in *Arabidopsis* mitochondria; (ii) these metabolites are present in the cytosol at very high concentrations (about 20 mM) (50), which are much higher than those of 2-oxoglutarate, malate, and oxaloacetate; (iii) both mitochondrial glutamate-oxaloacetate transaminase and malate dehydrogenase are involved in the regeneration of NAD^+ by GDC in mitochondria (51), and both mitochondrial and peroxisomal malate dehydrogenases are required for optimal photorespiration rates (52, 53); and (iv) as shown by the BAR *Arabidopsis* eFP Browser 2.0 (http:/bar.utoronto.ca),[7] AtUCP1 and AtUCP2 are expressed in many plant tissues, being more highly expressed in photosynthetic ones (Figs. S4 and S5). Interestingly, the expression of AtUCP1 is co-regulated with enzymes of the citric acid cycle, such as aconitase, isocitrate dehydrogenase, α-ketoglutarate dehydrogenase, and succinyl-CoA ligase, as well as with the peroxisomal transporter for NAD^+ (21, 22) (Fig. S6).

It is noteworthy that AtUCP1 (and AtUCP2) may also catalyze (i) the exchange between malate$_{in}$ and oxoglutarate$_{out}$ (*i.e.* the other mitochondrial membrane reaction of MAS) (Fig. 10) and (ii) an oxaloacetate$_{out}$/malate$_{in}$ exchange, which *per se* would result in export of the reducing equivalents of NADH from the mitochondria. However, these exchanges are also catalyzed by other *Arabidopsis* MCs, such as DTC, DIC1, DIC2, and DIC3 (23, 24), and the affinities of AtUCP1 and AtUCP2 for aspartate are much higher than those for the other substrates.

An additional hypothetical function of AtUCP1 and AtUCP2 in the photorespiratory glycolate pathway concerns the transfer of nitrogen equivalents across the mitochondrial membrane. During oxidative glycine decarboxylation by GDC in mitochondria, ammonia is released and reassimilated by the plastidial glutamine synthetase/glutamine oxoglutarate aminotransferase (GS/GOGAT) reaction. How ammonia released by GDC in mitochondria is shuttled to GS/GOGAT is still unknown, but it has been suggested that shuttling of amino acids across the mitochondrial membrane might be involved in this process (54). One possible route that would involve AtUCP1 and/or AtUCP2 would be incorporation of ammonia into 2-oxoglutarate by mitochondrial glutamate dehydrogenase, yielding glutamate, which is exported to the cytoplasm in counterexchange with external 2-oxoglutarate, thereby providing a new acceptor molecule for the glutamate dehydrogenase reaction. This hypothesis awaits experimental testing in future work.

Due to their broad substrate specificities, AtUCP1 (and AtUCP2) may be multifunctional and play further important physiological roles, depending on the metabolic conditions of the organ/tissue and the light/dark phase. For example, they might be involved in sulfur metabolism by exchanging cysteine sulfinate, cysteate, and cysteine with sulfate. Furthermore, in the dark, AtUCP1 (and AtUCP2) may catalyze the transport of glutamate into the mitochondria and the exit of aspartate to the cytosol, providing (together with the other enzymes of the malate aspartate shuttle) reducing equivalents in the form of NADH + H^+ to the mitochondrial respiratory chain.

Experimental procedures

Sequence analysis

BLAST and reciprocal BLAST were used to search for homologs of AtUCP1 and AtUCP2 (encoded by At3g54110 and At5g58970, respectively) in e!Ensamble and UniProt. Sequences were aligned with ClustalW.

Bacterial expression and purification of AtUCP1 and AtUCP2

PCR using complementary sequence-based primers was used to amplify the coding sequences of AtUCP1 from *A. thaliana* leaf cDNA and AtUCP2 from a custom-made synthetic gene (Invitrogen) with codons optimized for *E. coli*. The forward and reverse oligonucleotide primers contained the restriction sites NdeI and HindIII (AtUCP1) or XhoI and EcoRI (AtUCP2). The amplified gene fragments were cloned into pMW7 (AtUCP1) and pRUN (AtUCP2) vectors and transformed into *E. coli* TG1 cells (Invitrogen). Transformants were selected on LB (10 g/liter tryptone, 5 g/liter yeast extract, 5 g/liter NaCl, pH 7.4) plates containing 100 μg/ml ampicillin. All constructs were verified by DNA sequencing.

AtUCP1 and AtUCP2 were overexpressed as inclusion bodies in the cytosol of *E. coli* BL21(DE3) (AtUCP1) and BL21 CodonPlus(DE3)-RIL (AtUCP2) as described previously (55). Control cultures with the empty vector were processed in parallel. Inclusion bodies were purified on a sucrose density gradient (56) and washed at 4 °C, first with TE buffer (10 mM Tris-HCl, 1 mM EDTA, pH 7.0); once with a buffer containing 3% Triton X-114 (w/v), 1 mM EDTA, 10 mM PIPES (pH 7.0), and 10 mM Na_2SO_4; and finally three times with TE buffer (57). The inclusion body proteins were solubilized in 2% lauric acid, 10 mM PIPES (pH 7.0), and 3% Triton X-114 (AtUCP1) or 1.6% sarkosyl (w/v), 10 mM PIPES, pH 7.0, and 0.6% Triton X-114

[7] Please note that the JBC is not responsible for the long-term archiving and maintenance of this site or any other third party hosted site.

(AtUCP2). Unsolubilized material was removed by centrifugation (15,300 × *g* for 10 min).

Reconstitution of AtUCP1 and AtUCP2 into liposomes and transport measurements

The solubilized recombinant proteins were reconstituted into liposomes by cyclic removal of the detergent with a hydrophobic column of Amberlite beads (Bio-Rad), as described previously (41). The reconstitution mixture contained solubilized proteins (about 6 μg), 1% Triton X-114, 1.4% egg yolk phospholipids as sonicated liposomes, 10 mM substrate, 20 mM PIPES (pH 7.0), 1 mg of cardiolipin, and water to a final volume of 700 μl. These components were mixed thoroughly, and the mixture was recycled 13 times through a Bio-Beads SM-2 column pre-equilibrated with a buffer containing 10 mM PIPES (pH 7.0) and 50 mM NaCl and the substrate at the same concentration used in the starting mixture.

External substrate was removed from proteoliposomes on a Sephadex G-75 column pre-equilibrated with 10 mM PIPES and 50 mM NaCl, pH 7.0. Transport at 25 °C was initiated by adding the indicated radioactive substrates (American Radiolabeled Chemicals Inc. or PerkinElmer Life Sciences) to substrate-loaded (exchange) or empty (uniport) proteoliposomes. Transport was terminated by adding 20 mM pyridoxal 5′-phosphate and 20 mM bathophenanthroline, which in combination inhibit the activity of several MCs completely and rapidly (58–60). In controls, the inhibitors were added at the beginning together with the radioactive substrate according to the "inhibitor-stop" method (41). Finally, the external substrate was removed, and the radioactivity in the proteoliposomes was measured. The experimental values were corrected by subtracting control values. The initial transport rates were calculated from the radioactivity incorporated into proteoliposomes in the initial linear range of substrate transport. The kinetic constants K_m, V_{max}, and K_i were determined from Lineweaver–Burk and Dixon plots. For efflux measurements, proteoliposomes containing 5 mM internal aspartate or malate were loaded with 5 μM [^{14}C] aspartate and [^{14}C]malate, respectively, by carrier-mediated exchange equilibrium (61, 62). The external radioactivity was removed by passing the proteoliposomes through Sephadex G-75 columns pre-equilibrated with 50 mM NaCl. Efflux was started by adding unlabeled external substrate or buffer alone and terminated by adding the inhibitors indicated above.

Cloning and transient expression of GFP fusion constructs

For subcellular localization of AtUCP1 and AtUCP2, the AtUCP1-GFP and the AtUCP2-GFP fusion constructs were prepared. The *AtUCP1* coding sequence was amplified via Phusion High-Fidelity DNA Polymerase (New England Biolabs) using primers BH254 and BH255 (Table S4) and cloned with the Gibson Assembly Cloning Kit (New England Biolabs) into the expression vector pTKan (63) using the restriction sites ApaI and SacII. The GFP coding sequence for C-terminal GFP fusion was inserted via SacII and SpeI into the pTKan vector. The final vector contains AtUCP1 with a C-terminal GFP (AtUCP1-GFP) under the control of an optimized *Arabidopsis* ubiquitin-10 promoter (64) and the terminator of the *nos* gene from *Agrobacterium tumefaciens*. The *AtUCP2* coding sequence was amplified via Phusion High-Fidelity DNA Polymerase (Thermo Fisher Scientific) using primers UCP2_BPF and UCP2_BPR-s (Table S4) and cloned into pDONR207 vector by a BP recombination reaction with BP Clonase II enzyme mix (Invitrogen). The resulting entry clone was used for an LR recombination reaction by LR Clonase II enzyme mix (Invitrogen) with pK7FWG2 destination vector (65) to construct expression vector for the expression of AtUCP2-GFP under the control of the 35S promoter.

A. tumefaciens strain GV3101 (pMP90) (66) was transformed with the localization vectors (AtUCP1-GFP and AtUCP2-GFP) and the mitochondrial marker IVD-eqFP611 expressing the *Arabidopsis* IVD tagged at the C terminus with eqFP611 (67, 68). 5 ml of YPD medium (20 g/liter tryptone, 10 g/liter yeast extract, 20 g/liter glucose) was inoculated with positively transformed cells and grown overnight at 28 °C. Cells were harvested via centrifugation (10 min, 3000 × *g*) and resuspended in infiltration buffer (10 mM $MgCl_2$, 10 mM MES, pH 5.7, 100 μM acetosyringone) to an A_{600} of 0.5. *N. benthamiana* leaves of the same age were co-infiltrated with mitochondrial marker and corresponding AtUCP1 and AtUCP2 fusion proteins (69). Protoplasts were isolated 2 days after infiltration. Therefore, leaves were cut into 0.5 × 0.5-cm pieces and incubated in Protoplast Digestion Solution (1.5% (w/v) cellulase R-10, 0.4% (w/v) macerozyme R-10, 0.4 M mannitol, 20 mM KCl, 20 mM MES, pH 5.6, 10 mM $CaCl_2$, 0.1% (w/v) BSA) for 2 h at 30 °C. Isolated protoplasts were resuspended in W5 solution (154 mM NaCl, 125 mM $CaCl_2$, 5 mM KCl, 2 mM MES, pH 5.6) and directly used for microscopy. Protoplasts were observed using a Zeiss LSM 780 confocal microscope and Zeiss ZEN software. The following excitation/emission wavelength settings were used: GFP (488 nm/490–550 nm), IVD-eqFP611 (561 nm/580–625 nm), and chlorophyll A (488 nm/640–710 nm). Pictures were processed using Fiji software (75) and Adobe Photoshop CS6 (Adobe Systems).

Isolation, generation, and molecular characterization of single- and double-knockout mutants of ucp1 and ucp2

T-DNA insertion lines for At*UCP1* (SAIL_536G01, referred to as *ucp1* (37)) and At*UCP2* (SALK_080188, referred to as *ucp2*) were obtained from the ABRC. To identify homozygous T-DNA insertion lines, genomic DNA was extracted and genotyped using gene-specific primer pairs (DG8/DG9 for *ucp1* and DG6/DG5 for *ucp2*) and a primer pair for T-DNA/gene junction (DG9/SAIL-LBa for *ucp1* and DG6/SALK-LBa1 for *ucp2*) (Table S4). The position of the T-DNA was checked by sequencing. Homozygous *ucp1* and *ucp2* were further propagated. To generate double mutants (referred to as dKO), homozygous *ucp1* and *ucp2* were crossed. Heterozygous plants were selected by PCR in the T1 generation. After self crossing, dKO were selected by PCR and further propagated.

Total RNA was extracted from wildtype, mutant, and transgenic *Arabidopsis* plants using the guanidinium thiocyanate-phenol-chloroform method (70) and subjected after DNase treatment (RQ1 RNase-Free DNase, Promega) to cDNA synthesis (Superscript II Rnase H- reverse transcriptase, Invitrogen). Gene expression of *AtUCP1* and *AtUCP2* were analyzed using gene-specific primer pairs. The following primer sets

were used: DG23/DG24 for At*UCP1* and DG25/DG26 for *AtUCP2* (Table S4). As a control for cDNA quality and quantity, a cDNA fragment of an actin gene (ACT7, At5g09810) was amplified using ML167 and ML168. PCR conditions were as follows: 94 °C for 2 min, followed by cycles of 94 °C for 30 s, 58 °C for 45 s, 72 °C for 60 s, and a final extension for 2 min. Products were visualized on an ethidium bromide–stained 1% agarose gel.

Metabolite profiling

To obtain a broad overview of the major pathways of central metabolism, an established GC-MS–based metabolite profiling method was used to quantify the relative metabolite levels in the *Arabidopsis* rosette (~50 mg fresh weight). The extraction, derivatization, standard addition, and sample injection were performed exactly as described previously (71). This analysis allowed the determination of 46 different compounds, representing the main classes of primary metabolites (*i.e.* amino acids, organic acids, and sugars).

Other methods

Proteins were analyzed by SDS-PAGE and stained with Coomassie Blue dye. The identity of the bacterially expressed, purified AtUCP1 and AtUCP2 was assessed by MALDI-TOF mass spectrometry of trypsin digests of the corresponding band excised from Coomassie-stained gels (25, 72). The amount of purified AtUCP1 and AtUCP2 proteins was estimated by laser densitometry of stained samples using carbonic anhydrase as a protein standard (73). The amount of protein incorporated into liposomes was measured as described (74) and was about 25% of protein added to the reconstitution mixture. K^+-diffusion potentials were generated by adding valinomycin (1.5 μg/mg phospholipid) to proteoliposomes in the presence of K^+ gradients. For the formation of an artificial ΔpH (acidic outside), nigericin (50 ng/mg phospholipid) was added to proteoliposomes in the presence of an inwardly directed K^+ gradient.

Author contributions—M.M., L.P., A.R.F., A.P.W., and F.P. conceptualization; M.M., L.D., D.G., T.O., B.H., L.P., and D.V.M. methodology; A.R.F., A.P.W., and F.P. supervision.

References

1. Palmieri, F., Pierri, C. L., De Grassi, A., Nunes-Nesi, A., and Fernie, A. R. (2011) Evolution, structure and function of mitochondrial carriers: a review with new insights. *Plant J.* **66,** 161–181 CrossRef Medline
2. Palmieri, F. (2013) The mitochondrial transporter family SLC25: identification, properties and physiopathology. *Mol. Aspects Med.* **34,** 465–484 CrossRef Medline
3. Palmieri, F. (2014) Mitochondrial transporters of the SLC25 family and associated diseases: a review. *J. Inherit. Metab. Dis.* **37,** 565–575 CrossRef Medline
4. Saraste, M., and Walker, J. E. (1982) Internal sequence repeats and the path of polypeptide in mitochondrial ADP/ATP translocase. *FEBS Lett.* **144,** 250–254 CrossRef Medline
5. Palmieri, F. (1994) Mitochondrial carrier proteins. *FEBS Lett.* **346,** 48–54 CrossRef Medline
6. Pebay-Peyroula, E., Dahout-Gonzalez, C., Kahn, R., Trézéguet, V., Lauquin, G. J.-M., and Brandolin, G. (2003) Structure of mitochondrial ADP/ATP carrier in complex with carboxyatractyloside. *Nature* **426,** 39–44 CrossRef Medline
7. Ruprecht, J. J., Hellawell, A. M., Harding, M., Crichton, P. G., McCoy, A. J., and Kunji, E. R. S. (2014) Structures of yeast mitochondrial ADP/ATP carriers support a domain-based alternating-access transport mechanism. *Proc. Natl. Acad. Sci. U.S.A.* **111,** E426–E434 CrossRef Medline
8. Palmieri, F., and Pierri, C. L. (2010) Mitochondrial metabolite transport. *Essays Biochem.* **47,** 37–52 CrossRef Medline
9. Palmieri, F., and Monné, M. (2016) Discoveries, metabolic roles and diseases of mitochondrial carriers: a review. *Biochim. Biophys. Acta* **1863,** 2362–2378 CrossRef Medline
10. Haferkamp, I., Hackstein, J. H. P., Voncken, F. G. J., Schmit, G., and Tjaden, J. (2002) Functional integration of mitochondrial and hydrogenosomal ADP/ATP carriers in the *Escherichia coli* membrane reveals different biochemical characteristics for plants, mammals and anaerobic chytrids. *Eur. J. Biochem.* **269,** 3172–3181 CrossRef Medline
11. Leroch, M., Neuhaus, H. E., Kirchberger, S., Zimmermann, S., Melzer, M., Gerhold, J., and Tjaden, J. (2008) Identification of a novel adenine nucleotide transporter in the endoplasmic reticulum of *Arabidopsis*. *Plant Cell* **20,** 438–451 CrossRef Medline
12. Linka, N., Theodoulou, F. L., Haslam, R. P., Linka, M., Napier, J. A., Neuhaus, H. E., and Weber, A. P. M. (2008) Peroxisomal ATP import is essential for seedling development in *Arabidopsis thaliana*. *Plant Cell* **20,** 3241–3257 CrossRef Medline
13. Arai, Y., Hayashi, M., and Nishimura, M. (2008) Proteomic identification and characterization of a novel peroxisomal adenine nucleotide transporter supplying ATP for fatty acid β-oxidation in soybean and *Arabidopsis*. *Plant Cell* **20,** 3227–3240 CrossRef Medline
14. Kirchberger, S., Tjaden, J., and Neuhaus, H. E. (2008) Characterization of the *Arabidopsis* Brittle1 transport protein and impact of reduced activity on plant metabolism. *Plant J.* **56,** 51–63 CrossRef Medline
15. Rieder, B., and Neuhaus, H. E. (2011) Identification of an *Arabidopsis* plasma membrane-located ATP transporter important for anther development. *Plant Cell* **23,** 1932–1944 CrossRef Medline
16. Gigolashvili, T., Geier, M., Ashykhmina, N., Frerigmann, H., Wulfert, S., Krueger, S., Mugford, S. G., Kopriva, S., Haferkamp, I., and Flügge, U.-I. (2012) The *Arabidopsis* thylakoid ADP/ATP carrier TAAC has an additional role in supplying plastidic phosphoadenosine 5′-phosphosulfate to the cytosol. *Plant Cell* **24,** 4187–4204 CrossRef Medline
17. Palmieri, L., Santoro, A., Carrari, F., Blanco, E., Nunes-Nesi, A., Arrigoni, R., Genchi, F., Fernie, A. R., and Palmieri, F. (2008) Identification and characterization of ADNT1, a novel mitochondrial adenine nucleotide transporter from *Arabidopsis*. *Plant Physiol.* **148,** 1797–1808 CrossRef Medline
18. Stael, S., Rocha, A. G., Robinson, A. J., Kmiecik, P., Vothknecht, U. C., and Teige, M. (2011) *Arabidopsis* calcium-binding mitochondrial carrier proteins as potential facilitators of mitochondrial ATP-import and plastid SAM-import. *FEBS Lett.* **585,** 3935–3940 CrossRef Medline
19. Monné, M., Miniero, D. V., Obata, T., Daddabbo, L., Palmieri, L., Vozza, A., Nicolardi, M. C., Fernie, A. R., and Palmieri, F. (2015) Functional characterization and organ distribution of three mitochondrial ATP-Mg/P_i carriers in *Arabidopsis thaliana*. *Biochim. Biophys. Acta* **1847,** 1220–1230 CrossRef Medline
20. Palmieri, F., Rieder, B., Ventrella, A., Blanco, E., Do, P. T., Nunes-Nesi, A., Trauth, A. U., Fiermonte, G., Tjaden, J., Agrimi, G., Kirchberger, S., Paradies, E., Fernie, A. R., and Neuhaus, H. E. (2009) Molecular identification and functional characterization of *Arabidopsis thaliana* mitochondrial and chloroplastic NAD^+ carrier proteins. *J. Biol. Chem.* **284,** 31249–31259 CrossRef Medline
21. Bernhardt, K., Wilkinson, S., Weber, A. P. M., and Linka, N. (2012) A peroxisomal carrier delivers NAD^+ and contributes to optimal fatty acid degradation during storage oil mobilization. *Plant J.* **69,** 1–13 CrossRef Medline
22. Agrimi, G., Russo, A., Pierri, C. L., and Palmieri, F. (2012) The peroxisomal NAD^+ carrier of *Arabidopsis thaliana* transports coenzyme A and its derivatives. *J. Bioenerg. Biomembr.* **44,** 333–340 CrossRef Medline
23. Picault, N., Palmieri, L., Pisano, I., Hodges, M., and Palmieri, F. (2002) Identification of a novel transporter for dicarboxylates and tricarboxylates in plant mitochondria: bacterial expression, reconstitution, functional

characterization, and tissue distribution. *J. Biol. Chem.* **277,** 24204–24211 CrossRef Medline

24. Palmieri, L., Picault, N., Arrigoni, R., Besin, E., Palmieri, F., and Hodges, M. (2008) Molecular identification of three *Arabidopsis thaliana* mitochondrial dicarboxylate carrier isoforms: organ distribution, bacterial expression, reconstitution into liposomes and functional characterization. *Biochem. J.* **410,** 621–629 CrossRef Medline
25. Hoyos, M. E., Palmieri, L., Wertin, T., Arrigoni, R., Polacco, J. C., and Palmieri, F. (2003) Identification of a mitochondrial transporter for basic amino acids in *Arabidopsis thaliana* by functional reconstitution into liposomes and complementation in yeast. *Plant J.* **33,** 1027–1035 CrossRef Medline
26. Palmieri, L., Todd, C. D., Arrigoni, R., Hoyos, M. E., Santoro, A., Polacco, J. C., and Palmieri, F. (2006) *Arabidopsis* mitochondria have two basic amino acid transporters with partially overlapping specificities and differential expression in seedling development. *Biochim. Biophys. Acta* **1757,** 1277–1283 CrossRef Medline
27. Palmieri, L., Arrigoni, R., Blanco, E., Carrari, F., Zanor, M. I., Studart-Guimaraes, C., Fernie, A. R., and Palmieri, F. (2006) Molecular identification of an *Arabidopsis S*-adenosylmethionine transporter: analysis of organ distribution, bacterial expression, reconstitution into liposomes, and functional characterization. *Plant Physiol.* **142,** 855–865 CrossRef Medline
28. Bouvier, F., Linka, N., Isner, J.-C., Mutterer, J., Weber, A. P. M., and Camara, B. (2006) Arabidopsis SAMT1 defines a plastid transporter regulating plastid biogenesis and plant development. *Plant Cell* **18,** 3088–3105 CrossRef Medline
29. Hamel, P., Saint-Georges, Y., de Pinto, B., Lachacinski, N., Altamura, N., and Dujardin, G. (2004) Redundancy in the function of mitochondrial phosphate transport in *Saccharomyces cerevisiae* and *Arabidopsis thaliana*. *Mol. Microbiol.* **51,** 307–317 CrossRef Medline
30. Palmieri, L., Pardo, B., Lasorsa, F. M., del Arco, A., Kobayashi, K., Iijima, M., Runswick, M. J., Walker, J. E., Saheki, T., Satrústegui, J., and Palmieri, F. (2001) Citrin and aralar1 are Ca^{2+}-stimulated aspartate/glutamate transporters in mitochondria. *EMBO J.* **20,** 5060–5069 CrossRef Medline
31. Fiermonte, G., Palmieri, L., Todisco, S., Agrimi, G., Palmieri, F., and Walker, J. E. (2002) Identification of the mitochondrial glutamate transporter: bacterial expression, reconstitution, functional characterization, and tissue distribution of two human isoforms. *J. Biol. Chem.* **277,** 19289–19294 CrossRef Medline
32. Klingenberg, M., and Winkler, E. (1985) The reconstituted isolated uncoupling protein is a membrane potential driven H^+ translocator. *EMBO J.* **4,** 3087–3092 Medline
33. Nicholls, D. G. (2006) The physiological regulation of uncoupling proteins. *Biochim. Biophys. Acta.* **1757,** 459–466 CrossRef Medline
34. Vozza, A., Parisi, G., De Leonardis, F., Lasorsa, F. M., Castegna, A., Amorese, D., Marmo, R., Calcagnile, V. M., Palmieri, L., Ricquier, D., Paradies, E., Scarcia, P., Palmieri, F., Bouillaud, F., and Fiermonte, G. (2014) UCP2 transports C4 metabolites out of mitochondria, regulating glucose and glutamine oxidation. *Proc. Natl. Acad. Sci. U.S.A.* **111,** 960–965 CrossRef Medline
35. Borecký, J., Maia, I. G., Costa, A. D., Jezek, P., Chaimovich, H., de Andrade, P. B., Vercesi, A. E., and Arruda, P. (2001) Functional reconstitution of *Arabidopsis thaliana* plant uncoupling mitochondrial protein (AtPUMP1) expressed in *Escherichia coli*. *FEBS Lett.* **505,** 240–244 CrossRef Medline
36. Vercesi, A. E., Borecký, J., de Godoy Maia, I., Arruda, P., Cuccovia, I. M., and Chaimovich, H. (2006) Plant uncoupling mitochondrial proteins. *Annu. Rev. Plant Biol.* **57,** 383–404 CrossRef Medline
37. Sweetlove, L. J., Lytovchenko, A., Morgan, M., Nunes-Nesi, A., Taylor, N. L., Baxter, C. J., Eickmeier, I., and Fernie, A. R. (2006) Mitochondrial uncoupling protein is required for efficient photosynthesis. *Proc. Natl. Acad. Sci. U.S.A.* **103,** 19587–19592 CrossRef Medline
38. Parsons, H. T., Christiansen, K., Knierim, B., Carroll, A., Ito, J., Batth, T. S., Smith-Moritz, A. M., Morrison, S., McInerney, P., Hadi, M. Z., Auer, M., Mukhopadhyay, A., Petzold, C. J., Scheller, H. V., Loqué, D., and Heazlewood, J. L. (2012) Isolation and proteomic characterization of the *Arabidopsis* Golgi defines functional and novel components involved in plant cell wall biosynthesis. *Plant Physiol.* **159,** 12–26 CrossRef Medline
39. Nikolovski, N., Rubtsov, D., Segura, M. P., Miles, G. P., Stevens, T. J., Dunkley, T. P. J., Munro, S., Lilley, K. S., and Dupree, P. (2012) Putative glycosyltransferases and other plant Golgi apparatus proteins are revealed by LOPIT proteomics. *Plant Physiol.* **160,** 1037–1051 CrossRef Medline
40. Palmieri, L., Palmieri, F., Runswick, M. J., and Walker, J. E. (1996) Identification by bacterial expression and functional reconstitution of the yeast genomic sequence encoding the mitochondrial dicarboxylate carrier protein. *FEBS Lett.* **399,** 299–302 CrossRef Medline
41. Palmieri, F., Indiveri, C., Bisaccia, F., and Iacobazzi, V. (1995) Mitochondrial metabolite carrier proteins: purification, reconstitution, and transport studies. *Methods Enzymol.* **260,** 349–369 CrossRef Medline
42. Brand, M. D., and Esteves, T. C. (2005) Physiological functions of the mitochondrial uncoupling proteins UCP2 and UCP3. *Cell Metab.* **2,** 85–93 CrossRef Medline
43. Jaburek, M., and Garlid, K. D. (2003) Reconstitution of recombinant uncoupling proteins: UCP1, -2, and -3 have similar affinities for ATP and are unaffected by coenzyme Q10. *J. Biol. Chem.* **278,** 25825–25831 CrossRef Medline
44. Fiermonte, G., Dolce, V., David, L., Santorelli, F. M., Dionisi-Vici, C., Palmieri, F., and Walker, J. E. (2003) The mitochondrial ornithine transporter: bacterial expression, reconstitution, functional characterization, and tissue distribution of two human isoforms. *J. Biol. Chem.* **278,** 32778–32783 CrossRef Medline
45. Monné, M., Miniero, D. V., Daddabbo, L., Robinson, A. J., Kunji, E. R. S., and Palmieri, F. (2012) Substrate specificity of the two mitochondrial ornithine carriers can be swapped by single mutation in substrate binding site. *J. Biol. Chem.* **287,** 7925–7934 CrossRef Medline
46. Fiermonte, G., Palmieri, L., Dolce, V., Lasorsa, F. M., Palmieri, F., Runswick, M. J., and Walker, J. E. (1998) The sequence, bacterial expression, and functional reconstitution of the rat mitochondrial dicarboxylate transporter cloned via distant homologs in yeast and *Caenorhabditis elegans*. *J. Biol. Chem.* **273,** 24754–24759 CrossRef Medline
47. Cavero, S., Vozza, A., del Arco, A., Palmieri, L., Villa, A., Blanco, E., Runswick, M. J., Walker, J. E., Cerdán, S., Palmieri, F., and Satrústegui, J. (2003) Identification and metabolic role of the mitochondrial aspartate-glutamate transporter in Saccharomyces cerevisiae. *Mol. Microbiol.* **50,** 1257–1269 CrossRef Medline
48. Dry, I. B., Dimitriadis, E., Ward, A. D., and Wiskich, J. T. (1987) The photorespiratory hydrogen shuttle: synthesis of phthalonic acid and its use in the characterization of the malate/aspartate shuttle in pea (*Pisum sativum*) leaf mitochondria. *Biochem. J.* **245,** 669–675 CrossRef Medline
49. Noguchi, K., and Yoshida, K. (2008) Interaction between photosynthesis and respiration in illuminated leaves. *Mitochondrion* **8,** 87–99 CrossRef Medline
50. Winter, H., Robinson, D. G., and Heldt, H. W. (1994) Subcellular volumes and metabolite concentrations in spinach leaves. *Planta* **193,** 530–535 CrossRef
51. Journet, E. P., Neuburger, M., and Douce, R. (1981) Role of glutamate-oxaloacetate transaminase and malate dehydrogenase in the regeneration of NAD for glycine oxidation by spinach leaf mitochondria. *Plant Physiol.* **67,** 467–469 CrossRef Medline
52. Cousins, A. B., Pracharoenwattana, I., Zhou, W., Smith, S. M., and Badger, M. R. (2008) Peroxisomal malate dehydrogenase is not essential for photorespiration in *Arabidopsis* but its absence causes an increase in the stoichiometry of photorespiratory CO_2 release. *Plant Physiol.* **148,** 786–795 CrossRef Medline
53. Lindén, P., Keech, O., Stenlund, H., Gardeström, P., and Moritz, T. (2016) Reduced mitochondrial malate dehydrogenase activity has a strong effect on photorespiratory metabolism as revealed by ^{13}C labelling. *J. Exp. Bot.* **67,** 3123–3135 CrossRef Medline
54. Linka, M., and Weber, A. P. M. (2005) Shuffling ammonia between mitochondria and plastids during photorespiration. *Trends Plant Sci.* **10,** 461–465 CrossRef Medline
55. Fiermonte, G., Walker, J. E., and Palmieri, F. (1993) Abundant bacterial expression and reconstitution of an intrinsic membrane-transport protein from bovine mitochondria. *Biochem. J.* **294,** 293–299 CrossRef Medline

56. Elia, G., Fiermonte, G., Pratelli, A., Martella, V., Camero, M., Cirone, F., and Buonavoglia, C. (2003) Recombinant M protein-based ELISA test for detection of antibodies to canine coronavirus. *J. Virol. Methods* **109,** 139–142 CrossRef Medline
57. Agrimi, G., Russo, A., Scarcia, P., and Palmieri, F. (2012) The human gene SLC25A17 encodes a peroxisomal transporter of coenzyme A, FAD and NAD^+. *Biochem. J.* **443,** 241–247 CrossRef Medline
58. Palmieri, L., Lasorsa, F. M., Iacobazzi, V., Runswick, M. J., Palmieri, F., and Walker, J. E. (1999) Identification of the mitochondrial carnitine carrier in *Saccharomyces cerevisiae*. *FEBS Lett.* **462,** 472–476 CrossRef Medline
59. Castegna, A., Scarcia, P., Agrimi, G., Palmieri, L., Rottensteiner, H., Spera, I., Germinario, L., and Palmieri, F. (2010) Identification and functional characterization of a novel mitochondrial carrier for citrate and oxoglutarate in *S. cerevisiae*. *J. Biol. Chem.* **285,** 17359–17370 CrossRef Medline
60. Di Noia, M. A., Todisco, S., Cirigliano, A., Rinaldi, T., Agrimi, G., Iacobazzi, V., and Palmieri, F. (2014) The human SLC25A33 and SLC25A36 genes of solute carrier family 25 encode two mitochondrial pyrimidine nucleotide transporters. *J. Biol. Chem.* **289,** 33137–33148 CrossRef Medline
61. Marobbio, C. M. T., Di Noia, M. A., and Palmieri, F. (2006) Identification of a mitochondrial transporter for pyrimidine nucleotides in *Saccharomyces cerevisiae*: bacterial expression, reconstitution and functional characterization. *Biochem. J.* **393,** 441–446 CrossRef Medline
62. Fiermonte, G., Paradies, E., Todisco, S., Marobbio, C. M. T., and Palmieri, F. (2009) A novel member of solute carrier family 25 (SLC25A42) is a transporter of coenzyme A and adenosine 3′,5′-diphosphate in human mitochondria. *J. Biol. Chem.* **284,** 18152–18159 CrossRef Medline
63. Krebs, M., Held, K., Binder, A., Hashimoto, K., Den Herder, G., Parniske, M., Kudla, J., and Schumacher, K. (2012) FRET-based genetically encoded sensors allow high-resolution live cell imaging of Ca^{2+} dynamics. *Plant J. Cell Mol. Biol.* **69,** 181–192 CrossRef
64. Grefen, C., Donald, N., Hashimoto, K., Kudla, J., Schumacher, K., and Blatt, M. R. (2010) A ubiquitin-10 promoter-based vector set for fluorescent protein tagging facilitates temporal stability and native protein distribution in transient and stable expression studies. *Plant J.* **64,** 355–365 CrossRef Medline
65. Karimi, M., Inzé, D., and Depicker, A. (2002) GATEWAY vectors for *Agrobacterium*-mediated plant transformation. *Trends Plant Sci.* **7,** 193–195 CrossRef Medline
66. Koncz, C., and Schell, J. (1986) The promoter of TL-DNA gene 5 controls the tissue-specific expression of chimaeric genes carried by a novel type of *Agrobacterium* binary vector. *Mol. Gen. Genet.* **204,** 383–396 CrossRef
67. Höfgen, R., and Willmitzer, L. (1988) Storage of competent cells for *Agrobacterium* transformation. *Nucleic Acids Res.* **16,** 9877 CrossRef Medline
68. Forner, J., and Binder, S. (2007) The red fluorescent protein eqFP611: application in subcellular localization studies in higher plants. *BMC Plant Biol.* **7,** 28 CrossRef Medline
69. Waadt, R., and Kudla, J. (2008) *In planta* visualization of protein interactions using bimolecular fluorescence complementation (BiFC). *CSH Protoc.* **2008,** pdb.prot4995 CrossRef Medline
70. Chomczynski, P., and Sacchi, N. (1987) Single-step method of RNA isolation by acid guanidinium thiocyanate-phenol-chloroform extraction. *Anal. Biochem.* **162,** 156–159 CrossRef Medline
71. Lisec, J., Schauer, N., Kopka, J., Willmitzer, L., and Fernie, A. R. (2006) Gas chromatography mass spectrometry-based metabolite profiling in plants. *Nat. Protoc.* **1,** 387–396 CrossRef Medline
72. Palmieri, L., Agrimi, G., Runswick, M. J., Fearnley, I. M., Palmieri, F., and Walker, J. E. (2001) Identification in *Saccharomyces cerevisiae* of two isoforms of a novel mitochondrial transporter for 2-oxoadipate and 2-oxoglutarate. *J. Biol. Chem.* **276,** 1916–1922 CrossRef Medline
73. Indiveri, C., Iacobazzi, V., Giangregorio, N., and Palmieri, F. (1998) Bacterial overexpression, purification, and reconstitution of the carnitine/acylcarnitine carrier from rat liver mitochondria. *Biochem. Biophys. Res. Commun.* **249,** 589–594 CrossRef Medline
74. Porcelli, V., Fiermonte, G., Longo, A., and Palmieri, F. (2014) The human gene SLC25A29, of solute carrier family 25, encodes a mitochondrial transporter of basic amino acids. *J. Biol. Chem.* **289,** 13374–13384 CrossRef Medline
75. Schindelin, J., Arganda-Carreras, I., Frise, E., Kaynig, V., Longair, M., Pietzsch, T., Preibisch, S., Rueden, C., Saalfeld, S., Schmid, B., Tinevez, J. Y., White, D. J., Hartenstein, V., Eliceiri, K., Tomancak, P., and Cardona, A. (2012) Fiji: an open-source platform for biological-image analysis. *Nat. Methods* **9,** 676–682 CrossRef Medline

Uncoupling proteins 1 and 2 (UCP1 and UCP2) from *Arabidopsis thaliana* are mitochondrial transporters of aspartate, glutamate, and dicarboxylates

Magnus Monné, Lucia Daddabbo, David Gagneul, Toshihiro Obata, Björn Hielscher, Luigi Palmieri, Daniela Valeria Miniero, Alisdair R. Fernie, Andreas P. M. Weber and Ferdinando Palmieri

J. Biol. Chem. 2018, 293:4213-4227.
doi: 10.1074/jbc.RA117.000771 originally published online January 25, 2018
